Removal of pharmaceuticals through UV-C/Performic acid advanced oxidation process: Kinetics and identification of reactive species

Christelle Nabintu Kajoka, Stephan Brosillon, Corine Reibel, Yacine Khadija Diop, Marcos Oliveira, Vincent Rocher, Ghassan Chebbo, Johnny Gasperi, Julien Le Roux

Journal of Hazardous Materials 495 (2025) 139016

Contents lists available at ScienceDirect

Journal of Hazardous Materials

journal homepage: www.elsevier.com/locate/jhazmat

Removal of pharmaceuticals through UV-C/Performic acid advanced oxidation process: Kinetics and identification of reactive species

Christelle Nabintu Kajoka [a], Stephan Brosillon [b], Corine Reibel [c], Yacine Khadija Diop [a], Marcos Oliveira [d], Vincent Rocher [d], Ghassan Chebbo [a], Johnny Gasperi [e], Julien Le Roux [a,*]

[a] LEESU, ENPC, Institut Polytechnique de Paris, Univ Paris Est Creteil, Marne-la-Vallée, France
[b] IEM - Institut Européen des Membranes, UMR 5635, Université de Montpellier, Montpellier F-34090, France
[c] PAC Chimie Balard, Univ Montpellier, CNRS, ENSCM, Montpellier, France
[d] SIAAP - Service Public de l'assainissement Francilien (SIAAP), Direction Innovation, Colombes F-92700, France
[e] GERS-LEE - Laboratoire Eau et Environnement, Université Gustave Eiffel, Bouguenais F-44344, France

HIGHLIGHTS

- UV-C/performic acid (PFA) is an emerging efficient advanced oxidation process for the removal of pharmaceuticals.
- Singlet oxygen ($^1O_2$) is generated via PFA autodecomposition and further amplified by UV-C/PFA.
- Hydroxyl ($HO^\bullet$) and peroxyl ($HCOO^\bullet$ and $HCOOO^\bullet$) radicals are the main reactive species generated under UV-C/PFA.
- $HO^\bullet$ radicals produced under UV-C/PFA are primarily generated by the background H_2O_2 concentration in the PFA solution.

GRAPHICAL ABSTRACT

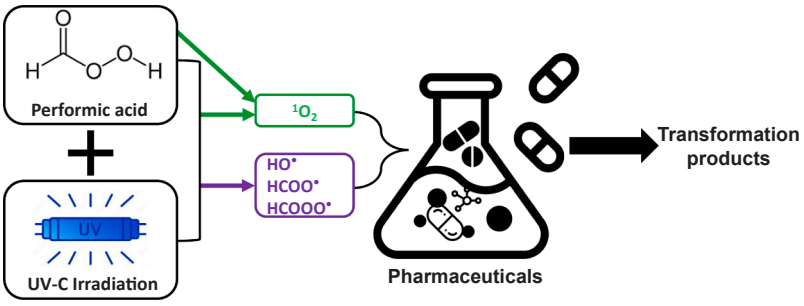

ARTICLE INFO

Keywords:
Peracid
Peracetic acid
Wastewater treatment
Transformation products
UV-C photolysis

ABSTRACT

Performic acid (PFA), widely recognized for its disinfectant properties in wastewater, shows selective and limited reactivity in oxidizing micropollutants. This study investigates the activation of PFA through UV-C photolysis to generate an advanced oxidation process (UV-C/PFA) and enhance the degradation of six pharmaceuticals: lidocaine, furosemide, sulfamethoxazole, diclofenac, acetaminophen, and carbamazepine. The synergy of UV-C photolysis with PFA enhances the removal of PFA-persistent pharmaceuticals. For instance, diclofenac, acetaminophen, and sulfamethoxazole, initially unreactive with PFA, were entirely degraded within ten minutes under UV-C/PFA in a phosphate buffer solution. This increased reactivity results from generated reactive species like hydroxyl ($HO^\bullet$), peroxyl ($R–O^\bullet$) radicals and singlet oxygen ($^1O_2$), confirmed by electron paramagnetic resonance, with $HO^\bullet$ primarily originating from the background H_2O_2 present in the PFA solution. While UV-C/PFA produced fewer $HO^\bullet$ than UV-C/H_2O_2, it has distinct advantages through the selective action of $^1O_2$ and $R–O^\bullet$ in degrading some pharmaceuticals. $^1O_2$ was also detected in the PFA solution and could explain its selective reactivity, especially with compounds containing reduced sulfur or tertiary amine groups. Overall, UV-C/PFA yields transformation products of lower molar mass compared to PFA, thus potentially increasing

* Corresponding author.
E-mail address: julien.le-roux@u-pec.fr (J. Le Roux).

https://doi.org/10.1016/j.jhazmat.2025.139016
Received 6 November 2024; Received in revised form 28 May 2025; Accepted 20 June 2025

mineralization. In wastewater effluent, UV-C/PFA improved pharmaceutical degradation, though scavenging effects by wastewater constituents reduced removal rates.

1. Introduction

The quality of surface water is increasingly deteriorating due to microbiological and chemical pollution from wastewater discharge. Conventional wastewater treatment plants (WWTPs) were not originally designed to efficiently remove this type of pollution, which has sparked interest in implementing additional (chemical or physical) treatments to improve the quality of discharged wastewater. Chlorine and ozone, while commonly used to remove microorganisms and micropollutants from water and wastewater, can also react with organic and inorganic compounds in water and generate disinfection by-products (DBPs). Some of these DBPs are known to be cytotoxic or genotoxic [50], and some can even be carcinogenic [42].

Peracids, specifically performic and peracetic acids (PFA and PAA, respectively), are gaining attention as alternative disinfectants because they form very few DBPs compared to traditional disinfectants [25,31,39] and are easy to implement technically at existing WWTPs [34]. While PAA was the first peracid proposed for wastewater disinfection nearly 50 years ago [4,40], PFA is garnering increased interest due to its demonstrated superior effectiveness and lower operational costs compared to PAA in removing *Escherichia coli* and enterococci during wastewater treatment [39,53]. In addition, its effectiveness in disinfection has been proven against a broad spectrum of microorganisms, including bacteria, viruses, spores, antibiotic-resistant bacteria, mycobacteria, and microscopic fungi [10,22,31,47]. Although PFA is used as an alternative wastewater disinfectant at full scale in Europe [53,56], its ability to degrade organic micropollutants (OMPs) that are consistently present in wastewater and known to have adverse effects [6,63] has been scarcely investigated. For instance, Gagnon et al., [21] studied the degradation of eight pharmaceuticals (six parent compounds: clofibric acid, ibuprofen, naproxen, triclosan, carbamazepine, diclofenac, and two metabolites: salicylic acid and 2-hydroxy-ibuprofen) from primary-treated wastewater by PFA and demonstrated poor reactivity (average removal rate < 8 %). Additionally, Ragazzo et al., [53] found that PFA had a weak oxidation power towards organic substances commonly found in wastewater, such as phenols and hormones like estrone. More recently, Nabintu Kajoka et al., [46] studied the removal of model organic compounds and pharmaceuticals by PFA, revealing the selective reactivity of PFA with reduced-sulfur moieties (total removal of ranitidine, 3-mercaptophenol, and benzenethiol in less than 1 min in a phosphate buffer solution) and deprotonated nitrogen-containing compounds (lidocaine, ranitidine) in both phosphate buffer solution and wastewater effluent. Based on the low reactivity of PFA with most pharmaceuticals, this study also demonstrated that PFA is generally a weaker oxidant compared to common oxidants such as ozone.

To enhance the removal rate of recalcitrant pharmaceuticals, UV-C photolysis can activate PFA to generate reactive species through a PFA-based advanced oxidation process (AOP). This approach, previously investigated for PAA (UV-C/PAA), resulted in an increased removal rate of organic compounds, attributed to the production of reactive radical species such as hydroxyl ($HO^{\bullet}$) and peroxyl ($R–O^{\bullet}$) radicals from the homolytic cleavage of PAA [2,8,27]. Therefore, this study investigates, for the first time, the potential benefits of coupling UV-C photolysis with PFA (UV-C/PFA) to enhance the reactivity of pharmaceuticals in phosphate buffer solution and wastewater effluent, using kinetic and removal rate approaches. As described previously [22], PFA exists as an equilibrium mixture of formic acid, water, and two oxidants: PFA and H_2O_2. Thus, UV-C/PFA generates a background AOP (UV-C/H_2O_2), whose contribution to the removal of pharmaceuticals by UV-C/PFA is investigated alongside a comparison of the two processes. In this study, the kinetic and removal rate approaches were investigated for six pharmaceuticals: lidocaine (LID), furosemide (FUR), diclofenac (DCF), acetaminophen (ACT), sulfamethoxazole (SMX) and carbamazepine (CBZ), chosen due to their consistent detection in Parisian wastewater discharges [24], and their previously studied reactivity with PFA [46]. Except for LID and FUR, the other four pharmaceuticals exhibited very low reactivity with PFA.

The first necessary step involved evaluating the photolysis of PFA under UV-C irradiation, including its light absorption and quantum yield, and comparing it with PAA, as UV-C/PAA serves as the reference for comparing the two peracid-based AOPs. In addition, the reactive species responsible for pharmaceutical degradation under UV-C/PFA were qualitatively and systematically evaluated. This study also investigated the influence of initial pH on the reaction kinetics and degradation mechanisms of two pharmaceuticals: one PFA-reactive compound (lidocaine) and one less reactive compound (diclofenac).

To the best of the authors' knowledge, this study is the first to highlight the benefits of UV-C/PFA for pharmaceutical oxidation and systematically investigate the photolysis behavior of PFA during wastewater treatment.

2. Materials and methods

2.1. Chemical reagents

All reagents were used in their as-received state without additional purification ($\geq$ 98 % purity for most reagents except for H_2O_2 (50 %) and phosphoric acid (85 %)). Pharmaceutical stock solutions were prepared in methanol (0.01–0.13 M), and their working solutions were obtained by dilution in deionized water (Milli-Q, 18 MΩ·cm). The PAA solution (38–40 % w/w) was a ready-to-use solution from Sigma-Aldrich. On the other hand, the PFA solutions were prepared in the laboratory by reacting formic acid (99 % purity) with H_2O_2 (50 % purity), following the method established previously [46,48]. The concentration of the peracid stock solutions was meticulously and periodically checked and found to contain, by weight, 19.2 ± 1.2 % of PFA (+ 19.5 ± 1.4 % of H_2O_2 and ~ 26 % of formic acid) or 28.4 ± 2.7 % of PAA (+ 4.3 ± 0.4 % of H_2O_2), using the iodometric titration method [12,56]. Due to its instability, the PFA stock solution was stored at −20 °C after preparation, while the PAA stock solution was stored at 4°C. For specific details regarding the purity and suppliers of other reagents, refer to Text S1 in the Supporting Information (SI).

2.2. Collimated beam experiments

UV-C photolysis and AOP experiments (including UV-C/PFA, UV-C/PAA, and UV-C/H_2O_2) were conducted using a custom-made quasi-collimated beam apparatus equipped with three 16 W low-pressure mercury vapor lamps (Philips, Eindhoven, Netherlands, Figure S1, SI). These lamps emit at a principal monochromatic wavelength of 254 nm. The collimated beam apparatus was used to determine the photodegradation kinetic rate constants of peracids and pharmaceuticals, as well as the removal rates of pharmaceuticals. The average UV-C intensity was determined with atrazine chemical actinometry (details described in SI, Text S2). The UV-C lamp was pre-heated for at least 30 min before each experiment to maintain stable light intensity, and continuous magnetic stirring was provided to ensure the reactor was thoroughly mixed at room temperature (~ 20°C).

2.3. UV-C photolysis of PFA and PAA

PFA and PAA solutions were prepared at different concentrations in

deionized (DI) water without pH adjustment (at pH levels of 3.8 and 5.9, respectively, for PFA and PAA) and in a 10 mM phosphate buffer solution (PBS) at pH levels of 7.1, 7.7 and 9.2. A precise volume of peracid was injected individually into 200 mL of DI water or PBS under stirring in a crystallizer to achieve each initial concentration.

As a crucial step, the molar absorption coefficients at 254 nm (ε_{254}) of PFA (1.3 $\times 10^{-2}$ M) and PAA (1.6 $\times 10^{-2}$ M) in DI water (pH 3.8 and 5.9, respectively, for PFA and PAA) and PBS (pH 9.2) were determined by using the Beer-Lambert law. This included measuring the total absorbance of peracid solutions containing H_2O_2, subtracting the H_2O_2 absorbance to isolate the specific absorbance of the peracid, and then dividing by the initial molar concentration of the peracid (Eq. (1)):

$$\varepsilon_{254} = \frac{A_{peracid} - A_{H_2O_2}}{[peracid]_0 \times L} \quad (1)$$

Where ε_{254} is the molar absorption coefficient of PFA or PAA ($M^{-1}.cm^{-1}$), A is the absorbance of peracid solution or pure H_2O_2 solution at 254 nm obtained after monitoring a blank with DI water or PBS depending on the solvent used for the preparation of the peracid solution (cm^{-1}), $[peracid]_0$ is the initial molar concentration of PFA or PAA (M), and L is the optical path length (1 cm).

In addition, the UV-C photolysis rate constants for PFA (29 μM) and PAA (23 μM) were determined both in DI water (without pH adjustment) and in a 10 mM PBS at pH levels of 7.1 and 7.7 to mimic a range of environmental conditions encountered in wastewater treatment. To determine the photolysis rate constants (Eq. (2)) and the quantum yield (Eq. (3)) of peracids, direct UV-C photolysis was performed with tert-butyl alcohol (TBA, 10 mM) added at the beginning of the reaction as an $HO^\bullet$ scavenger [8]. The solution was then placed under the collimated beam apparatus within five seconds after peracid addition. For these experiments, the fluence rate was 0.3 $mW.cm^{-2}$ (1.1 $\times$ 10^{-7} $Einstein.L^{-1}.s^{-1}$, conversion detailed in Text S2). Samples were taken at various intervals to quantify the residual peracid concentration using the N, N′-diethyl-p-phenylenediamine (DPD) colorimetric method [46], as the iodometric titration method is not suitable for low peracid concentrations. The photolytic decomposition of peracids followed first-order kinetics (Eq. (2)):

$$\frac{d\,[peracid]}{dt} = - k_{peracid} \times [peracid] \quad (2)$$

Where $k_{peracid}$ is the observed first-order photolytic rate constant for PFA or PAA (min^{-1}), and [peracid] is the mass concentration of PFA or PAA ($mg.L^{-1}$).

In addition, the quantum yields of both peracids were calculated based on Eq. (3) (assuming the peracid is the only significant absorber of light), as previously described in the literature [8]:

$$\Phi_{254} = \frac{(k_{UV-C/peracid+TBA} - k_{peracid} - k_{UV-C/H_2O_2}) \times A}{I_{254} \times (1 - 10^{-A \times L}) \times \varepsilon_{254}} \quad (3)$$

Where Φ_{254} is the quantum yield at 254 nm ($mol.Einstein^{-1}$), $k_{UV\text{-}C/peracid+TBA}$, $k_{peracid}$, $k_{UV\text{-}C/H2O2}$ are the rate constants experimentally determined (s^{-1}) for the direct UV-C photolysis of the peracids (after quenching with TBA), peracid autodecomposition, and photodegradation of H_2O_2 contained in the peracid solution, respectively. I_{254}, referred to as fluence, is the incident light intensity ($Einstein.L^{-1}.s^{-1}$), and L is the light path in water (3 cm in this study). Note that here, $A = (\varepsilon_{PFA^0} \times PFA^0) + (\varepsilon_{PFA^-} \times PFA^-) + (\varepsilon_{H_2O_2} \times H_2O_2)$ (cm^{-1}). All experiments were performed at least in duplicate.

2.4. Photodegradation experiments

The PBS (10 mM, pH 7.0) containing each pharmaceutical (LID, FUR, DCF, ACT, SMX and CBZ at 1 μM) was prepared in a 100 mL reactor. Then, a precise volume of PFA working solution was added to the reactor under stirring to achieve an initial concentration of 500 μM (31 $mg.L^{-1}$). Within five seconds after the PFA addition, the reactor was placed under the collimated beam apparatus to initiate the AOP experiments. To evaluate the contribution of the background H_2O_2 concentration present in the PFA solution, control experiments were conducted with UV-C/H_2O_2 by substituting the PFA solution with pure H_2O_2 solution (892 μM = 30 $mg.L^{-1}$, corresponding to the background H_2O_2 concentration in 500 μM = 31 $mg.L^{-1}$ of PFA). In addition, control experiments were carried out with UV-C photolysis (without PFA or pure H_2O_2) to assess its contribution to the degradation of pharmaceuticals by different AOPs.

Furthermore, the impact of the PFA initial concentration was evaluated on the production of $HO^\bullet$, given that these radicals were generated via UV-C/PAA [8,75,76,2] and expected to be also generated via UV-C/PFA. The $HO^\bullet$ production was indirectly measured through the degradation of a quenching probe compound, parachlorobenzoic acid (pCBA, 1 μM), in 10 mM PBS (pH 7.0) with four different PFA concentrations: 16, 161, 500 and 806 μM. Additionally, the contribution of H_2O_2 to the production of $HO^\bullet$ within the UV-C/peracid system was assessed. The kinetic rate constants of pCBA were thus compared between three systems: UV-C/PFA (500 μM, 31 $mg.L^{-1}$), UV-C/PAA (408 μM, 31 $mg.L^{-1}$) and UV-C/H_2O_2 (H_2O_2 concentrations equivalent to that in peracid solution: 892 μM and 147 μM as present in the PFA and PAA solutions, respectively). To check the contribution of each process individually on the $HO^\bullet$ production, control pCBA degradation experiments were conducted by UV-C photolysis alone or with each oxidant alone (PFA or PAA or H_2O_2 without UV-C photolysis).

Furthermore, the contribution of some potentially produced reactive species to the degradation of pharmaceuticals by UV-C/PFA (500 μM of PFA) was evaluated on three pharmaceuticals (LID, DCF, and ACT at 1 μM) through quenching experiments using TBA and MeOH at 200 mM each.

In addition, the effect of pH was also evaluated during the oxidation of LID and DCF by UV-C/PFA (1 μM of pharmaceutical and 500 μM of PFA). This evaluation involved adjusting the initial pH of the PBS to five levels: 2.0, 5.0, 7.0, 9.0, and 11.0.

For all experiments, the reaction time in the reactor was 30 min for UV-C photolysis, PFA, and H_2O_2. It varied between 3 and 10 min for AOP experiments (UV-C/PFA and UV-C/H_2O_2), except for CBZ, which consistently underwent a 30 min oxidation across all processes due to its lower reactivity. For these experiments, the fluence was 0.5 ± 0.01 $mW.cm^{-2}$ (2.3 ± 0.03 × 10^{-7} $Einstein.L^{-1}.s^{-1}$). At each UV-C dose interval, 1.5 mL of the sample was withdrawn from the reactor, injected into an amber vial containing excess sodium thiosulfate ($[Na_2S_2O_3]_0/[PFA]_0$ = 7) to stop the reaction and stored at 4°C before being analyzed (part 2.7). All experiments were conducted at least in duplicate, and the average results are presented.

Pharmaceuticals and pCBA photodegradation followed pseudo-first-order kinetics, and the observed kinetic rate constants (min^{-1}) were calculated following Eq. (4).

$$\frac{d[compound]}{dt} = \ln \frac{[compound]}{[compound]_0} = - k_{obs} \times [compound] \quad (4)$$

Where k_{obs} is the observed pseudo-first-order kinetic rate constant for pharmaceuticals or pCBA with each process (UV-C/PFA, UV-C/PAA, UV-C/H_2O_2, UV-C photolysis and each oxidant alone for pCBA), [compound] and $[compound]_0$ are the molar concentrations of pharmaceuticals or pCBA at time t and initial time, respectively.

2.5. Identification of different reactive species produced by UV-C/PFA

The identification of reactive species produced by UV-C/PFA and potentially involved in the photodegradation of pharmaceuticals was assessed in PBS (pH 7.0) via kinetic experiments using Electron Paramagnetic Resonance (EPR) and mass spectrometry analysis. In this first experimental setup, 5,5-dimethyl-1-pyrroline-N-oxide (DMPO) and

2,2,6,6-tetramethyl-4-piperidol (TMP) were used as free radicals and singlet oxygen ($^1O_2$) trapping agents, respectively. Specifically, DMPO (2 and 50 mM) and TMP (50 mM) were oxidized by UV-C/PFA (1 mM, 62 mg.L^{-1}) and UV-C/H_2O_2 (1.8 mM, 61 mg.L^{-1}, corresponding to the background H_2O_2 concentration in the PFA solution). Moreover, specific DMPO experiments employed TBA (5 and 50 mM) and MeOH (100 mM) as quenching agents to distinguish HO$^\bullet$ and some other organic radicals. In the second experimental setup, HO$^\bullet$ production was indirectly quantified by monitoring the degradation of pCBA (1 μM) under UV-C/PFA (500 μM PFA), while $^1O_2$ generation was assessed using 9,10-diphenylanthracene (DPA, 0.1 mM) and furfuryl alcohol (FFA, 1.2 mM) under UV-C/PFA (1.0 mM PFA). The UV-C fluence was 0.5 mW.cm^{-2} for TMP, DPA, and FFA experiments and 1.2 mW.cm^{-2} for DMPO experiments, as the latter were conducted with a specific apparatus that did not allow for controlling the fluence. Control experiments were conducted with PFA and/or H_2O_2.

2.6. Removal of pharmaceuticals by UV-C/PFA in wastewater effluent

The photodegradation of the six pharmaceuticals was assessed in treated biological wastewater effluent collected from the Seine Amont WWTP located in Valenton, France. Samples were collected directly before the discharge channel and filtered in the laboratory through a 0.45 μm glass fiber filter (Whatman). The WWTP processes were previously described [48]. The wastewater quality parameters were as follows (mean ± standard deviation over three samples): pH 7.9 ± 0.1, total suspended solids 5.5 ± 2.8 mg.L^{-1}, UV absorbance at 254 nm (UV_{254}) 1.1 ± 0.6, nitrite 0.6 ± 0.1 mgN.L^{-1}, ammonium 1.6 ± 1.0 mg/L, phosphate 3.1 ± 0.9 mgP.L^{-1}, dissolved organic carbon 8.1 ± 0.7 mgC.L^{-1}, and temperature 22.9 ± 0.6 °C. The six pharmaceuticals (LID, FUR, DCF, ACT, SMX, and CBZ) were spiked into treated wastewater effluent at an individual concentration of 1 μg.L^{-1} in addition to their initial concentration. The effluent was then subjected to batch oxidation experiments without any pH adjustment. A precise volume of PFA stock solution was added to achieve an initial concentration of 161 μM (10 mg.L^{-1}) under constant stirring, followed by immediate UV-C irradiation within five seconds. To determine the pharmaceutical removal rate, after 60 min, excess $Na_2S_2O_3$ ($[Na_2S_2O_3]_0/[PFA]_0 = 7$) was added to stop the reaction. Samples were then withdrawn and stored at 4 °C before being extracted and analyzed, as described in part 2.7. All experiments were conducted in triplicate to ensure accuracy.

2.7. Analytical methods

A high-performance liquid chromatography equipped with a diode array detector (HPLC-DAD, SPD-M20A, Shimadzu) was used to analyze pharmaceuticals in DI water and determine the kinetic rate constants. The analytical parameters, including stationary and mobile phases, elution gradient, and pharmaceutical-specific operating wavelengths with maximum UV absorbance, were previously documented [46]. For pCBA, the analytical method for pharmaceuticals was applied, using a maximum UV absorbance wavelength of 234 nm. All details concerning the analysis of atrazine, used to determine UV-C fluence, are provided in SI, Text S2.

The analysis of the six pharmaceuticals spiked into wastewater effluent was conducted using ultrahigh-performance liquid chromatography (UPLC) coupled with tandem mass spectrometry (MS/MS) employing a triple quadrupole detector (Acquity-TQD, Waters) equipped with an electrospray ionization (ESI) source. Samples were subjected to extraction using an automated solid-phase extraction (SPE) system (Dionex Autotrace 280, Thermo Scientific) using homemade multilayer SPE cartridges, as previously described [30,48]. Specific analytical parameters, including stationary and mobile phases, internal standards, elution gradient, ionization mode, and MS/MS acquisition parameters, were previously described [46].

A UPLC system, coupled to a high-resolution ion-mobility time-of-flight mass spectrometry (Vion IMS-QTof, Waters) equipped with an ESI source, was used to analyze pharmaceutical transformation products (TPs), DPA, FFA, and their respective TPs (DPA endoperoxide and 6-hydroxy(2 H)pyran-3(6 H)one). The analysis was performed in both negative and positive ionization modes, and mass spectra were acquired in HDMS^E (data independent analysis) mode to obtain low and high collision energy fragments. The instrument and methods were previously described [48].

The EPR spectra of reactive species were recorded in situ using a Bruker-Elexsys E500 spectrometer (Bruker, Germany) with an X Band frequency in continuous wave at room temperature. The settings for the EPR spectrometer were as follows: a center field of 3510 G, a sweep width of 100 G, a microwave frequency of 9.854 GHz, a microwave power of 20 mW, a receiver gain of 50 dB, a sweep time of 21 s, 1 G field modulation amplitude, and 100 KHz field modulation.

The absorption spectrum and the absorbance of all compounds were measured using a UV-Vis spectrometer (VWR Spectrophotometer UV-6300PC), and the pH of the solution was measured using a pH meter (VWR WTW-pH 3110 SenTix® 41).

3. Results and discussion

3.1. UV-C photolysis of peracids

To elucidate the degradation mechanisms of pharmaceuticals via UV-C/PFA, the photolysis of PFA at 254 nm was first investigated across three different pH levels. In experiments conducted in DI water (without pH regulation), the pH was 3.8, whereas in experiments conducted in PBS (10 mM), the pH was regulated to 7.1 and 7.7, and in these three conditions, the final pH decreased by less than 0.5 units. The UV-C photolysis of PFA followed first-order kinetics (Fig. 1a), consistent with its autodecomposition behavior [46]. In DI water at pH 3.8, the UV-C photolysis rate constant of PFA was 1.2 ± 0.03 × 10^{-1} min^{-1}, while in PBS, it increased up to 6.3 ± 1.2 × 10^{-1} and 5.8 ± 0.5 × 10^{-1} min^{-1}, respectively at pH 7.1 and 7.7. Compared to PFA autodecomposition, UV-C photolysis increased PFA decay by a factor of 9–14 at the three tested pH levels ($k_{autodecomposition}$ = 8.7 ± 0.1 × 10^{-3} min^{-1} in DI water at pH 3.8, 6.7 ± 0.4 × 10^{-2} and 6.5 ± 0.5 × 10^{-2} min^{-1} in PBS respectively at pH 7.1 and 7.7, [46]). Therefore, the increased PFA decay under UV-C photolysis could be attributed to the co-existence of three mechanisms: autodecomposition, direct UV-C photolysis, and decomposition by the produced reactive species. Based on the reaction chain proposed for UV-C/PAA [8], the PFA photolysis could occur through a chain of radical reactions expressed by Eq. 5.

$$HC(=O)O_2H \xrightarrow{hv} HC(=O)O^\bullet + HO^\bullet \quad (a)$$

$$H_2O_2 \xrightarrow{hv} 2HO^\bullet \quad (b)$$

$$HC(=O)O^\bullet \rightarrow H^\bullet + CO_2 \quad (c)$$

$$HC(=O)O_2H + HO^\bullet \rightarrow HC(=O)OH + HOO^\bullet \quad (d)$$

$$HC(=O)O_2H + HO^\bullet \rightarrow HC(=O)O_2^\bullet + H_2O \quad (e)$$

$$HC(=O)O_2H + HO^\bullet \rightarrow HC(=O)^\bullet + O_2 + H_2O \quad (f)$$

$$H^\bullet + O_2 \rightarrow HO_2^\bullet \quad (g)$$

$$HC(=O)O_2H + HC(=O)O^\bullet \rightarrow HC(=O)O_2^\bullet + HC(=O)OH \quad (h)$$

$$HO^\bullet + HO_2^\bullet \rightarrow H_2O + {}^1O_2 \quad (i)$$

$$2HC(=O)O_2H \rightarrow 2\,HC(=O)OH + {}^1O_2 \quad (j)$$

Eq. 5: Chemical reaction chain for the photolysis of PFA (adapted from

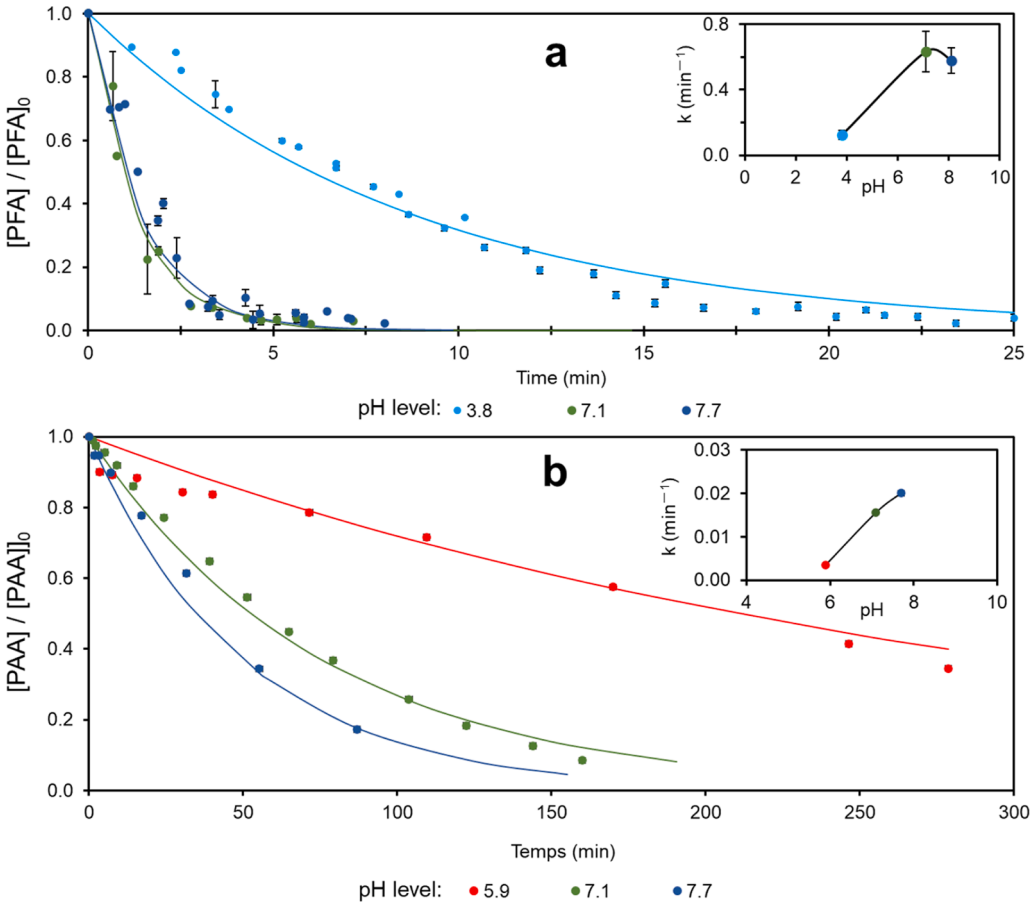

Fig. 1. Photolytic decomposition of PFA (a) and PAA (b) in 10 mM phosphate buffer solution (PBS) at various initial pH levels. The runs at pH 3.8 and 5.9 were carried out in DI water without pH regulation. [PFA or PAA]$_0$ = 1.8 ± 0.3 mg.L^{-1} (equivalent to 29 μM of PFA and 23 μM of PAA).

Cai et al., [9])

Initially, UV-C light induces the homolytic cleavage of the O−O bond in the PFA molecule, producing a formyloxy radical (HC(=O)O$^{\bullet}$) and HO$^{\bullet}$ (a). In addition, the UV-C photolysis of H_2O_2 is an important source of HO$^{\bullet}$ (b). The HC(=O)O$^{\bullet}$ can decompose into a hydrogen radical (H$^{\bullet}$) and carbon dioxide (CO_2, c), while HO$^{\bullet}$ can attack PFA to generate formic acid (HC(=O)OH) and hydroperoxyl radical (HOO$^{\bullet}$, d) or performyloxy radical (HC(=O)O$_2^{\bullet}$) and H_2O (e) or formyl radical (HC(=O)$^{\bullet}$), oxygen (O_2), and H_2O (f). Moreover, the generated H$^{\bullet}$ (c) can react with O_2 (f) to form a hydroperoxyl radical (HO$_2^{\bullet}$, g), while HC(=O)O$^{\bullet}$ can react with PFA, leading to the formation of HC(=O)O$_2^{\bullet}$ and HC(=O)OH (h). Additionally, HO$^{\bullet}$ can react with HO$_2^{\bullet}$ (i), producing H_2O and $^1O_2$. The formation of $^1O_2$ also occurs via the autodecomposition of PFA (Eq. 5j and part 3.2) through an ionic mechanism [59,61].

Furthermore, the UV-C photolysis of PAA at 254 nm was also conducted for comparison purposes. Under acidic conditions (Fig. 1b, pH 5.9 resulting from the addition of PAA in DI water), the UV-C photolysis of PAA primarily relied on its slow autodecomposition, with a rate constant value ($k_{photolysis}$ = 3.4 × 10^{-3} min^{-1}) closely aligned with the autodecomposition rate constant value previously reported at the same pH ($k_{autodecomposition}$ = 3.6 × 10^{-3} min^{-1}, [46]). However, under neutral and alkaline conditions, besides the autodecomposition, both UV-C photolysis and decomposition by reactive species contributed to PAA decay, with $k_{photolysis}$ values of 1.6 × 10^{-2} min^{-1} (pH 7.1) and 2.0 ± 0.06 × 10^{-2} min^{-1} (pH 7.7), approximately five times higher than $k_{autodecomposition}$ at pH 7.7 (3.1 × 10^{-3} min^{-1}, [46]).

Globally, the $k_{photolysis}$ for both PFA and PAA exhibited a similar trend to $k_{autodecomposition}$, with the decay occurring approximately five to six times faster under neutral and alkaline than under acidic conditions (Fig. 1). Thus, the higher $k_{photolysis}$ of PFA observed in neutral and alkaline conditions could be attributed to its increased molar UV absorption coefficient at λ= 254 nm in alkaline (ε_{PFA} = 12.5 ± 0.6 M^{-1}.cm^{-1} at pH 9.2) compared to acidic conditions (ε_{PFA} = 8.8 ± 0.3 M^{-1}.cm^{-1} at pH 3.8). At pH > pKa = 7.1, ε_{PFA} should stabilize due to the predominance of its deprotonated form (PFA$^-$) [46]. Nevertheless, the ε_{PAA} in acidic (8.3 ± 0.7 M^{-1}.cm^{-1} at pH 5.9) and alkaline (7.7 ± 0.5 M^{-1}.cm^{-1} at pH 9.2) conditions were quite similar, with the former closely matching the literature value (8.0 M^{-1}.cm^{-1}, pH 5.1), whereas the last being notably lower than the literature value (41.6 M^{-1}.cm^{-1}, pH 9.7, [9]), despite the higher $k_{photolysis}$ in alkaline conditions (Fig. 1). Moreover, the ε_{H2O2} at λ = 254 nm was determined to be 19.0 M^{-1}.cm^{-1}, in accordance with the literature (18.7 M^{-1}.cm^{-1}, [5]).

In addition, PFA was more susceptible to UV-C photolysis than PAA despite having nearly the same activation energy for decomposition: 95.4 kJ.mol^{-1} for PFA [61] and 92.1 kJ.mol^{-1} for PAA [72]. This higher $k_{photolysis}$ of PFA can be attributed to the elevated background concentration of H_2O_2 in the PFA solution (1.8 μM of H_2O_2 per μM of PFA solution vs. 0.4 μM of H_2O_2 per μM of PAA solution), which could lead to greater production of HO$^{\bullet}$ (part 3.3.1), subsequently accelerating the PFA decay (Eq. 5). Furthermore, this phenomenon is also corroborated by the higher apparent quantum yield (Φ) of PFA, which is 0.9 mol.Einstein^{-1} at pH 3.8 and 2.5 mol.Einstein^{-1} at pH 9.2, higher than the Φ of PAA (0.7 mol.Einstein^{-1} at pH 5.9). The Φ_{PAA} is lower than the previously reported values of 0.88 [76] and 1.20 mol.Einstein^{-1} [8], likely due to the lower fluence rate employed in the present study. Furthermore, the addition of TBA partially inhibited the UV-C photolysis of PFA and PAA, confirming peracid scavenging by HO$^{\bullet}$, with a more pronounced inhibitory effect observed under acidic conditions, as already reported for UV-C/PAA [8]. The reduced inhibitory effect of peracid photolysis under alkaline conditions after TBA addition is likely due to

the additional scavenging action of hydroxide ions (OH^-) on the generated radicals, such as $HO^•$, a mechanism previously documented [18]. Assuming that TBA scavenges only $HO^•$ and that $HO^•$ are primarily responsible for the indirect photolysis of peracids, the reaction kinetics between peracids and $HO^•$ were investigated (Text S3). The $k_{PFA/HO•}$ were 2.0×10^9 and 3.1×10^9 $M^{-1}.s^{-1}$, respectively, at pH 3.8 and 9.2, higher than the $k_{PAA/HO•}$ (2.9×10^8 $M^{-1}.s^{-1}$ at pH 5.9). This $k_{PAA/HO•}$ was also lower than the value (9.3×10^8 $M^{-1}.s^{-1}$ at pH 6.1) reported by Cai et al., [9], likely due to the lower fluence rate employed in the present study. Therefore, the $k_{PFA/HO•}$ are 1−2 orders of magnitude higher than $k_{PAA/HO•}$ and $k_{H2O2/HO•}$ (2.7×10^7 $M^{-1}.s^{-1}$ as mentioned in Buxton et al., [7] without specifying pH, which was measured to be 5.2 in the present study), indicating that $HO^•$ exhibits a stronger scavenging effect on PFA. To the best of our knowledge, this is the first study to report the Φ_{PFA} and $k_{PFA/HO•}$. These data and the reactions mentioned earlier (Eq. 5) highlight the complexity of radical mechanisms involved in the activation of PFA by UV-C photolysis, generating various reactive species ($HO^•$, R–$O^•$, and $^1O_2$) that may exhibit different reactivities. This underlines the necessity for experimental validation using other techniques like EPR to confirm the presence of some reactive species (part 3.2).

3.2. Identification of reactive species by electron paramagnetic resonance (EPR)

Several techniques enable the identification and quantification of reactive species in AOPs. They include physical (e.g., spectral measurement of chemiluminescence using a red-sensitive photomultiplier or a liquid nitrogen-cooled germanium diode detector), and chemical techniques using different probe compounds, 9-[2-(3-carboxy-9,10-diphenyl)anthryl]-6-hydroxy-3H-xanthen-3-ones for fluorescence detection [23,62], DPA [43,44], FFA [26], pCBA for spectroscopic and spectrophotometric detection, 2,2,6,6-tetramethylpiperidin and its derivatives (e.g., 2,2,6,6-tetramethyl-4-piperidinol and 2,2,6,6-tetramethyl-4-piperidone) for EPR detection. In the present study, in situ EPR measurement using spin trap compounds was chosen for two main reasons: first, it enables the detection of the two main hypothesized reactive species ($HO^•$ and $^1O_2$), and second, to the best of our knowledge, all studies focusing on the detection of reactive species in peracid systems, specifically peracetic acid, have employed this technique [2,18,33,36,37,57,66,68,70,73,74]. In this regard, free radicals and $^1O_2$ produced by PFA and UV-C/PFA were monitored using two probe compounds: DMPO and TMP, respectively. Additionally, to distinguish the free radicals, based on results on UV-C/PAA [18,32,8], TBA was used to selectively quench $HO^•$, while MeOH was used to quench both $HO^•$ and some R–$O^•$ [8,18,32], although no relevant data exists regarding the capability of MeOH to quench the R–$O^•$ produced by UV-C/PFA. In addition, the production of $^1O_2$ and $HO^•$ was also confirmed by spectroscopic detection (parts 3.2 for $^1O_2$ and 3.3.1 for $HO^•$).

After 5 min of reaction with DMPO, no radical signal was detected with PFA alone (Fig. 2a). However, characteristic peaks corresponding to $HO^•$ (DMPO–$HO^•$, with hyperfine splitting constants of $a_N = a_H =$ 14.9 G, a four-fold characteristic peak with intensities in the ratio 1:2:2:1) were observed with UV-C/PFA and UV-C/H_2O_2. For the same H_2O_2 concentration (1.8 mM = 61 mg.L^{-1}, equivalent to the background concentration in PFA solution), the peak intensities were higher under UV-C/H_2O_2 than UV-C/PFA, implying that the former produced more $HO^•$. This difference is likely due to the scavenging effect of formate ions (pKa = 3.75) present in the PFA solution, as the experiments were conducted in PBS at pH 7.1 ± 0.1. This finding is consistent with previous observations for UV-C/PAA and UV-C/H_2O_2, where the former produces fewer $HO^•$ despite the higher Φ_{PAA} (0.9 mol.Einstein^{-1}) than Φ_{H2O2} (0.5 mol.Einstein^{-1}), due to the scavenging effect of acetate ions and R–$O^•$ in UV-C/PAA [76]. Furthermore, the addition of TBA (5 mM) in both systems (UV-C/PFA and UV-C/H_2O_2) had the same effect: nearly total suppression of the $HO^•$ signal (referring to the peak-to-peak amplitude after adjusting the baseline to zero, Fig. 2a).

In addition, the intensity of $HO^•$ increased over time under UV-C/PFA (Fig. 2b), reaching maximum intensity at 6 min, then decreased from 6 to 8 min, and disappeared entirely at 10 min. The decrease in

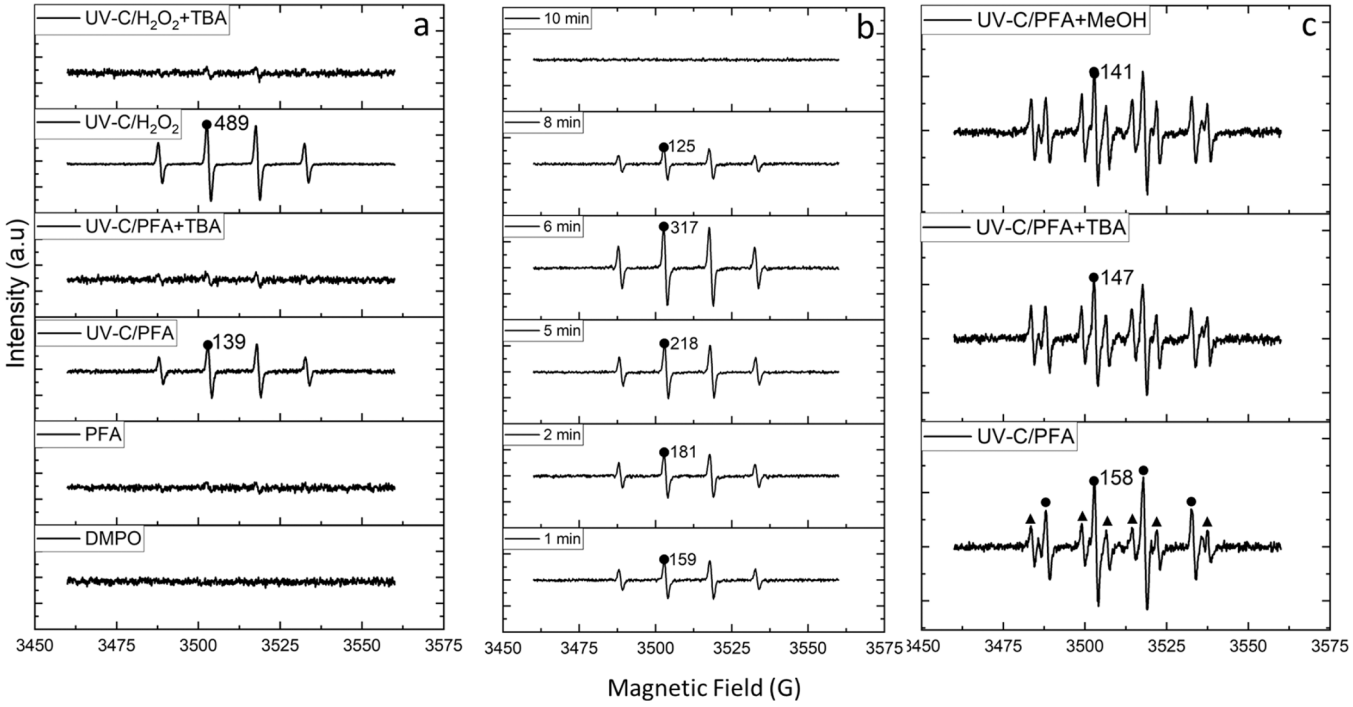

Fig. 2. Spin trapping EPR spectra of DMPO before and after oxidation by PFA, UV-C/PFA, UV-C/PFA + TBA, UV-C/H_2O_2 and UV-C/H_2O_2 + TBA (a), UV-C/PFA at different reaction times (b), and UV-C/PFA, UV-C/PFA + TBA, and UV-C/PFA + MeOH (c), with points corresponding to $HO^•$ and triangles to other organic radical signals (c). Conditions: [DMPO] = 2 mM for a and b, 50 mM for c, $[PFA]_0$ = 1 mM, $[H_2O_2]_0$ = 1.8 mM, $[TBA]_0$ = 5 mM for a and b, 50 mM for c, $[MeOH]_0$ = 100 mM for c, initial pH 7.1 ± 0.1. The intensity refers to the peak-to-peak amplitude after adjusting the baseline to zero and is in an arbitrary unit.

$HO^{\bullet}$ production over time likely results from the increased PFA decomposition and $HO^{\bullet}$ consumption through other radical reactions (Eq. 5). The evolution of $HO^{\bullet}$ production under UV-C/PFA can affect the removal of pharmaceuticals reactive with $HO^{\bullet}$. Furthermore, additional radical peaks were observed under UV-C/PFA when the initial concentration of DMPO was increased to 50 mM (Fig. 2c, peaks marked by triangles). These peaks exhibited the following hyperfine splitting constants: $a_N = 15.4$ G and $a_H = 23.0$ G, which could correspond to the primary R–$O^{\bullet}$, specifically $HCOO^{\bullet}$ and $HCOOO^{\bullet}$ (Fig. 2c). The proposition of $HCOO^{\bullet}$ and $HCOOO^{\bullet}$ as the primary formed R–$O^{\bullet}$ is based on their suggested presence in PFA-based AOPs [19] and the reactive radical structures previously suggested for UV-C/PAA [8,76]. Interestingly, the addition of TBA (50 mM) or MeOH (100 mM) slightly reduced the intensity of $HO^{\bullet}$and did not affect R–$O^{\bullet}$ (Fig. 2c). This suggests that while MeOH is commonly used as a scavenger for several types of reactive radicals, including $HO^{\bullet}$, it is not suitable to quench all R–$O^{\bullet}$ generated by UV-C/PFA. Some studies mentioned the use of 2,4-hexadiene instead of MeOH in PAA-based AOPs to achieve broader quenching results [32,76]. Further experiments are needed to evaluate the quenching impact of MeOH through UV-C/PFA (part 3.3.3). Therefore, the limited effect of TBA and MeOH on $HO^{\bullet}$, resulting in only a slight reduction of the $HO^{\bullet}$ signal, is attributed to the high concentration of DMPO (50 mM), which scavenges $HO^{\bullet}$ at a rate ($3.4–4.3 \times 10^9$ $M^{-1}.s^{-1}$, [1,20]) that surpasses the quenching efficiency of TBA (7.6×10^8 $M^{-1}.s^{-1}$, [18]) and MeOH (9.7×10^8 $M^{-1}.s^{-1}$, [18]). Furthermore, the generation of $HO^{\bullet}$ via UV-C/PFA was also confirmed by the observed oxidation of pCBA (Fig. 3).

Additionally, the $^1O_2$ signal (a third-fold characteristic peak with intensities in the ratio 1:1:1) corresponding to the 4-hydroxy-2,2,6,6-tetramethylpiperidin-1-oxyl (TEMPO), an oxidation product generated by the reaction between TMP and $^1O_2$ [14,45], was detected in both PFA and UV-C/PFA systems (Figure S2) with the intensity increasing over time (Figure S3), while no signal was observed in the TMP solution. A control experiment confirmed that phosphate ions did not affect the formation of $^1O_2$, as evidenced by the intensity comparison between

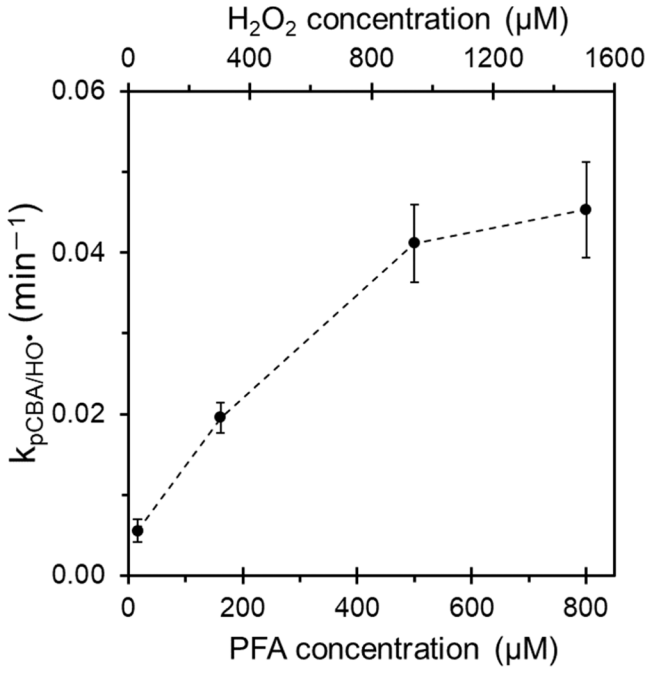

Fig. 3. Effect of PFA concentration on the rate constant of pCBA degradation by UV-C/PFA. Experimental conditions: $[pCBA]_0 = 1$ μM in phosphate buffer solution (10 mM, pH 7.0), $[PFA]_0 = 16–806$ μM, $[H_2O_2]_0 = 29–1\,439$ μM, 30 min of reaction, UV-C fluence = 0.5 ± 0.01 mW.cm^{-2} = $2.3 \pm 0.03 \times 10^{-7}$ Einstein. $L^{-1}.s^{-1}$.

experiments in DI water and PBS under identical conditions of PFA concentration and reaction time (Figure S3). These results suggest that $^1O_2$ was generated through PFA autodecomposition (Eq. 5j), consistent with prior findings on PAA [18]. Moreover, UV-C/PFA showed a significantly higher peak intensity, indicating enhanced $^1O_2$ formation via the reaction between $HO^{\bullet}$ and $HO_2^{\bullet}$ (Eq. 5i). $^1O_2$ formation was further investigated by oxidizing DPA and FFA under PFA and UV-C/PFA. This approach was explored due to the potential side reactions between TMP and radicals, such as $HO^{\bullet}$, which may reduce the EPR signal intensity [54]. The detection of DPA endoperoxide and 6-hydroxy(2 H)pyran-3(6 H)one (Figure S4a and b), specific TPs of DPA and FFA, formed via oxidation by $^1O_2$ [26,43,44], confirmed the generation of $^1O_2$. Their peak intensities increased over time, with higher levels observed in UV-C/PFA (Figure S4c and d), supporting the EPR results. Although FFA and DPA confirmed $^1O_2$ formation, their suitability as probes in PFA-based AOPs is limited. While FFA reacts faster with $HO^{\bullet}$ (1.5×10^{10} $M^{-1}.s^{-1}$, [77]) than with $^1O_2$ (1.0×10^8 $M^{-1}.s^{-1}$, [3]), compromising its selectivity, DPA has poor water solubility and is photosensitive [8,78,71]. Furthermore, anthracene-derived endoperoxides can photodecompose back to anthracene and other products [55], restricting their applicability in photo-AOPs. Given the limited selectivity and specificity of existing probes in peracid-based AOPs, improved and more specific $^1O_2$ probes are needed.

However, the $^1O_2$ produced through PFA autodecomposition can explain its selective reactivity with specific functional groups, such as reduced sulfur, aniline, deprotonated tertiary amine, and furan rings, as demonstrated previously [46]. $^1O_2$ is indeed known for its high reactivity towards compounds containing electron-rich sites, leading to electrophilic addition, single-electron transfer, or oxygen addition to heteroatoms, specifically nitrogen or sulfur [17,41,54]. In addition, $^1O_2$ also preferentially attacks the ortho and para positions of phenol rings due to the higher electron density at these sites, resulting from the ortho-para directing nature of the –OH group. This is in accordance with the increased reactivity of PFA with catechol and hydroquinone compared to resorcinol, as previously reported [46].

3.3. Degradation of organic compounds by UV-C/PFA

3.3.1. Quantification of $HO^{\bullet}$ produced through UV-C/PFA and UV-C/PAA

To determine the optimal PFA concentration for subsequent experiments, $HO^{\bullet}$ production through UV-C/PFA was investigated. $HO^{\bullet}$ are known for their non-selectivity and high oxidation efficiency toward numerous micropollutants [69], owing to their high redox potential of 2.8 V/ESH [49] and can be easily measured with probe compounds. Thus, $HO^{\bullet}$ were indirectly quantified using pCBA as the probe compound ($k_{pCBA/HO^{\bullet}} = 5.0 \times 10^9$ $M^{-1}.s^{-1}$, [58]) because previous studies have demonstrated that pCBA cannot be oxidized by the organic radicals produced specifically by PAA-based AOPs [15,65]. Due to the high reactivity of pCBA with $HO^{\bullet}$, its rapid degradation, expressed by a first-order rate constant (min^{-1}), serves as an indicator of $HO^{\bullet}$ abundance. Prior to quantifying $HO^{\bullet}$ generated by UV-C/PFA and UV-C/PAA, control experiments were performed to determine whether each process independently produced $HO^{\bullet}$. To this end, the degradation of pCBA (1 μM) was initially evaluated under UV-C photolysis and in the presence of individual oxidants (PFA or PAA or H_2O_2 at 31 mg.L^{-1}). The results showed that pCBA degradation by these processes was very low (Figure S5), near zero, with rate constants of $3.8 \pm 0.7 \times 10^{-3}$, $9.9 \pm 4.2 \times 10^{-4}$, $9.4 \pm 3.7 \times 10^{-4}$ and $6.8 \pm 0.4 \times 10^{-4}$ min^{-1} for UV-C photolysis, PFA, PAA and H_2O_2, respectively. This finding, in accordance with EPR results, confirms that in the present experimental conditions, none of these processes could individually produce $HO^{\bullet}$ and contradicts the assumption made in the literature that peracid disinfection relies on a radical mechanism involving reactive species such as $HO^{\bullet}$ [22,31,38,39,60]. Additionally, the lack of pCBA degradation by PFA suggests that the $^1O_2$ generated through PFA autodecomposition does not react with pCBA. Then, pCBA (1 μM) was oxidized by

UV-C/PFA using four PFA concentrations: 16, 161, 500, and 806 μM (equivalent to 1, 10, 31, and 50 mg.L^{-1}) under a UV-C fluence of 0.5 ± 0.01 mW.cm^{-2} (2.3 ± 0.03 × 10^{-7} Einstein.L^{-1}.s^{-1}). These PFA concentrations contained approximately equivalent mass concentrations of H_2O_2 (29, 288, 892, and 1 439 μM, equivalent to 1, 10, 30, and 49 mg.L^{-1}). Fig. 3 demonstrates that, under UV-C/PFA, the pCBA degradation increased with PFA concentration from 16 to 500 μM, after which it stabilized up to 806 μM. This increase in $HO^•$ production can be linked to the simultaneous increase of both PFA and background H_2O_2 concentration. However, the stabilization of $HO^•$ production at higher PFA concentrations (> 500 μM) can be attributed to scavenging effects resulting from potential side reactions between PFA or background H_2O_2 and the generated reactive species, including $HO^•$. This phenomenon is comparable to that occurring in the UV-C/H_2O_2 and UV-C/PAA processes (considering its UV-C/H_2O_2 background AOP), where high oxidant concentrations (e.g., > 0.59 mM of H_2O_2 or 0.10 mM of PAA) can act as active scavengers. Indeed, H_2O_2 and PAA are renowned for their strong reactivity with $HO^•$, with rate constants of $k_{H2O2/HO•}$ of 2.7 × 10^7 M^{-1}.s^{-1} at pH 5.2 [7] and $k_{PAA/HO•}$ of 2.9 × 10^8 M^{-1}.s^{-1} at pH 5.9, often leading to the formation of less reactive radicals such as $HO_2^•$ in the case of H_2O_2 [11,35]. As an increase in PFA concentration leads to an increase in H_2O_2 concentration (in the same ratio), it is worth considering the existence of an optimal H_2O_2 concentration in the UV-C/PFA process, as it has been observed in other AOPs such as UV-C/H_2O_2 [35,52] or ozone/H_2O_2 [13]. Thus, the excess H_2O_2 concentration might be photon flux dependent and could potentially lead to the consumption of the produced $HO^•$, subsequently decreasing $HO^•$ yield. Therefore, 500 μM of PFA (containing 892 μM of H_2O_2) was chosen as the optimal concentration for $HO^•$ production for the subsequent experiments.

Additionally, this experiment aimed to determine the contribution of H_2O_2 to $HO^•$ production through peracid-based AOPs. The production of $HO^•$ was thus compared between the UV-C/peracid (31 mg.L^{-1} of peracids = 500 μM of PFA and 408 μM of PAA) and UV-C/H_2O_2 systems (Fig. 4) at the H_2O_2 concentrations equivalent to that present in peracid solutions (i.e., 892 μM in PFA and 147 μM in PAA, respectively). The results demonstrated significantly higher pCBA degradation under UV-C/PFA than UV-C/PAA, and showed that $HO^•$ production under UV-C/H_2O_2 was comparable to that observed with UV-C/PFA and UV-C/PAA (Fig. 4).

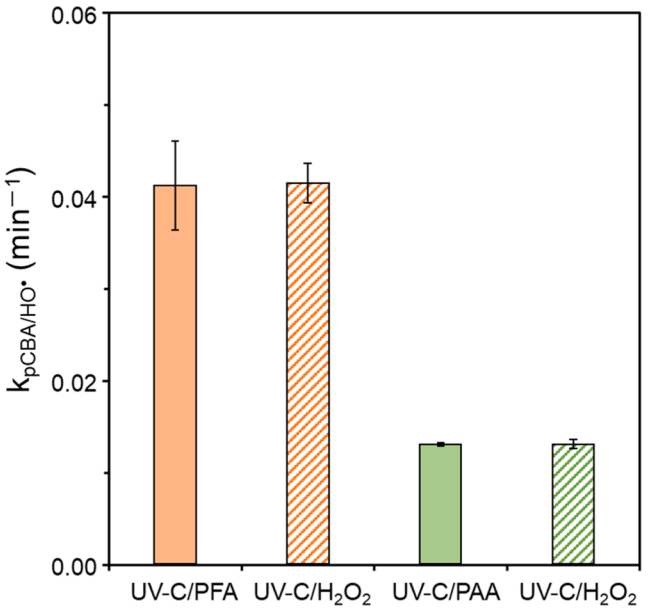

Fig. 4. Contribution of H_2O_2 on $HO^•$ production in UV-C/peracid system (through UV-C/H_2O_2 at equivalent concentrations of H_2O_2). $[pCBA]_0$ = 1 μM in phosphate buffer solution (10 mM, pH 7.0), $[PFA]_0$ = 500 μM ($[H_2O_2]_0$ = 892 μM), $[PAA]_0$ = 408 μM ($[H_2O_2]_0$ = 147 μM), 30 min of reaction, UV-C fluence = 0.5 ± 0.01 mW.cm^{-2} = 2.3 ± 0.03 × 10^{-7} Einstein.L^{-1}.s^{-1}.

The ratio between the kinetic rate constants for pCBA degradation under UV-C/PFA and UV-C/PAA is 4, which closely matches the ratio between the background concentrations of H_2O_2 in peracids, equivalent to 6. This suggests that $HO^•$ under UV-C/PFA or UV-C/PAA primarily originate from the photolysis of background H_2O_2 in the peracid solution, contrary to previous literature, which indicated that $HO^•$ production under UV-C/PAA mainly arise from PAA photolysis [75]. If PAA or PFA can indeed produce $HO^•$, these radicals are present in negligible amounts compared to the quantities produced by the background H_2O_2 concentration. As far as we know, this is the first time the contribution of H_2O_2 in UV-C/PFA or UV-C/PAA has been demonstrated and quantified in terms of $HO^•$ production. Therefore, $HO^•$ was produced more under UV-C/PFA than UV-C/PAA, as the H_2O_2 background concentration is higher in the PFA (~ 20 % w/w) than in the PAA (~ 4 % w/w) solution.

3.3.2. *Kinetic rate constants of pharmaceuticals under UV-C/PFA in phosphate buffer solution*

Six pharmaceuticals (LID, FUR, DCF, ACT, SMX and CBZ) at 1 μM were oxidized by UV-C/PFA (500 μM of PFA, UV-C fluence of 0.5 mW.cm^{-2} = 2.3 ± 0.03 × 10^{-7} Einstein.L^{-1}.s^{-1}) in PBS (10 mM, pH 7.0). The plot of ln([pharmaceutical]/[pharmaceutical]$_0$) vs. time resulted in a straight line (data not shown), confirming that the photolytic degradation of pharmaceuticals by UV-C/PFA followed apparent first-order kinetics. Pharmaceutical solutions contained 0.03–0.05 % MeOH. Although previous studies [16] indicated that MeOH may influence $HO^•$generation and thus affect AOP efficiency, the low concentration used in this study minimizes such effects. For instance, the kinetic rate constants for DCF degradation under UV-C/H_2O_2 closely align with literature values [29].

A control experiment with UV-C photolysis alone was conducted using the six pharmaceuticals and revealed kinetic rate constants (k_{UV-C}) varying between 1.4 ± 0.3 × 10^{-4} min^{-1} for CBZ and 2.9 ± 0.03 × 10^{-1} min^{-1} for DCF. Since UV-C/H_2O_2 is the primary source of $HO^•$ (part 3.3.1) in the UV-C/peracid system, a supplementary experiment was conducted by using pure H_2O_2 at the same concentration as that in the PFA solution (892 μM of H_2O_2 in 500 μM of PFA) to investigate its contribution to the degradation of pharmaceuticals. The k_{UV-C} values of DCF, SMX, and FUR were close to their $k_{UV-C/H2O2}$, indicating that direct UV-C photolysis played a significant role in their degradation compared to $HO^•$ produced from UV-C/H_2O_2 ($k_{UV-C/H2O2}$/k_{UV-C} ratio of 1.0, 1.1, and 1.3, respectively). The experiment also showed that CBZ degradation was due to $HO^•$ rather than direct UV-C photolysis ($k_{UV-C/H2O2}$/k_{UV-C} ratio of 30.3). Additionally, after 5 min of reaction under UV-C/PFA, DCF, SMX, FUR, and ACT exhibited degradation rates of ≥ 80.0 %, whereas their degradation was very low (~ 10.0 % after 30 min) with PFA alone. Under UV-C/PFA (5 min of reaction), LID was degraded at only 45 %, while CBZ displayed the lowest reactivity, with a degradation rate of < 4.0 %. Therefore, the UV-C/PFA kinetic rate constants for all six pharmaceuticals ranged from 4.8 ± 0.3 × 10^{-3} min^{-1} for CBZ to 5.5 ± 0.1 × 10^{-1} min^{-1} for ACT (Table 1). Compared to the k_{PFA} of these pharmaceuticals (Table 1, data obtained from Nabintu Kajoka et al., [46]), the $k_{UV-C/PFA}$ were approximately 22–171 times higher than k_{PFA}, except for LID, whose $k_{UV-C/PFA}$ was only 1.2 times higher. Therefore, a synergistic effect between UV-C photolysis and PFA was observed for all pharmaceuticals except LID. This increased reactivity of pharmaceuticals with UV-C/PFA is likely attributed to the generation of various reactive species resulting from the activation of PFA. For all the investigated pharmaceuticals, the $k_{UV-C/PFA}$/$k_{UV-C/H2O2}$ ratios ranged from 1.2 (CBZ) to 14.9 (FUR), confirming that, apart from the $HO^•$ generated from the background H_2O_2, other reactive species ($^1O_2$ and R–$O^•$) played a more significant role in the degradation of these pharmaceuticals. These additional reactive species reacted selectively with some pharmaceuticals, such as FUR, ACT, LID, and SMX, while exhibiting lower

Table 1
The pseudo-first-order rate constant (k_{obs}, min^{-1}) of pharmaceuticals under PFA (data from [46]), UV-C/PFA, UV-C/H_2O_2, and UV-C alone (this work). Experimental conditions: [pharmaceutical]$_0$ = 1 μM, [PFA]$_0$ = 500 μM, [H_2O_2]$_0$ = 892 μM in UV-C/H_2O_2 experiments, [PBS] = 10 mM, pH 7.10, 20 ± 1 °C, UV-C fluence = 0.5 ± 0.01 mW.cm^{-2} = 2.3 ± 0.03 × 10^{-7} Einstein.L^{-1}.s^{-1}.

Compounds	k_{PFA}	$k_{UV-C/PFA}$	k_{UV-C/H_2O_2}	k_{UV-C}	$\frac{k_{UV-C/PFA}}{k_{PFA}}$	$\frac{k_{UV-C/PFA}}{k_{UV-C/H_2O_2}}$	$\frac{k_{UV-C/PFA}}{k_{UV-C}}$	$\frac{k_{UV-C/H_2O_2}}{k_{UV-C}}$
LID	(9.3 ± 0.9) x10^{-2}	(1.1 ± 0.1) x10^{-1}	(2.6 ± 0.5) x10^{-2}	(1.3 ± 0.3) x10^{-4}	1.2	4.1	788.5	193.1
FUR	(1.2 ± 0.5) x10^{-2}	(3.8 ± 0.9) x10^{-1}	(2.5 ± 0.2) x10^{-2}	(2.0 ± 0.02) x10^{-2}	31.5	14.9	18.8	1.3
SMX	(4.0 ± 0.7) x10^{-3}	(3.3 ± 0.5) x10^{-1}	(1.1 ± 0.2) x10^{-1}	(1.2 ± 0.01) x10^{-1}	83.3	2.9	2.8	1.0
DCF	(4.0 ± 1.1) x10^{-3}	(4.8 ± 0.9) x10^{-1}	(3.3 ± 0.4) x10^{-1}	(2.9 ± 0.03) x10^{-1}	120.4	1.4	1.6	1.1
ACT	(3.2 ± 0.7) x10^{-3}	(5.5 ± 0.1) x10^{-1}	(9.4 ± 1.7) x10^{-2}	(1.6 ± 0.2) x10^{-3}	170.5	5.8	346.5	59.7
CBZ	(2.1 ± 0.3) x10^{-4}	(4.8 ± 0.3) x10^{-3}	(4.1 ± 0.2) x10^{-3}	(1.4 ± 0.3) x10^{-4}	22.5	1.2	35.3	30.3

reactivity towards CBZ and DCF, as evidenced by their low $k_{UV-C/PFA}$/-$k_{UV-C/H2O2}$ ratio (Table 1). Since HO$^{\bullet}$ are known for their non-selectivity, if they were the sole primary reactive species generated by UV-C/PFA, the k_{obs} for all pharmaceuticals would likely be within the same order of magnitude. However, no literature is currently available on UV-C/PFA; still, Cai et al., [9] studied the reactivity of six pharmaceuticals, including DCF and CBZ, with UV-C/PAA and found kinetic rate constants of 1.4 ± 0.03 and 8.3 ± 0.3 × 10^{-2} min^{-1}, respectively, which were higher than those observed for UV-C/PFA (4.76 ± 0.85 ×10^{-1} min^{-1} and 4.76 ± 0.32 ×10^{-3} min^{-1}, respectively). This difference may be attributed to the significantly higher fluence rate used in the study by Cai et al., [9] (2.1 × 10^{-6} Einstein.L^{-1}·s^{-1}) compared to that employed in the present study (3.4 ± 0.1 × 10^{-7} Einstein.L^{-1}·s^{-1}), which likely resulted in higher production of reactive species and/or also higher UV-C photolysis rates. Another study reported a k_{obs} of ~ 0.1 min^{-1} for DCF with UV-C/PAA, using a high light intensity (2.1 mW.cm^{-2} = 9.7 × 10^{-7} Einstein.L^{-1}·s^{-1}) [75].

In conclusion, the reactivity of all pharmaceuticals was influenced by either HO$^{\bullet}$ (based on $k_{UV-C/H2O2}/k_{UV-C}$ in this order: LID > ACT > FUR > CBZ > DCF, with the last two pharmaceuticals being less impacted) or additional reactive species (including $^1O_2$ and organic radicals, based on the $k_{UV-C/PFA}/k_{UV-C/H2O2}$ ratio: FUR > ACT > LID > SMX > DCF ~ CBZ). Therefore, the oxidation of pharmaceuticals by UV-C/PFA is a complex, molecule-dependent process that involves direct UV-C photolysis, oxidation by PFA, and, in some cases, oxidation by various reactive species, including HO$^{\bullet}$, R–O$^{\bullet}$, and $^1O_2$. This experiment highlights the need to investigate further the contribution of these reactive species to the degradation of pharmaceuticals (part 3.3.3).

3.3.3. *Contribution of reactive species in the degradation of pharmaceuticals by UV-C/PFA*

As observed previously (part 3.3.2), UV-C/PFA enhances the reactivity of pharmaceuticals due to the formation of various reactive species (HO$^{\bullet}$, R–O$^{\bullet}$, and $^1O_2$). Kinetic experiments using TBA and MeOH as quenching agents were conducted to quantify the contribution of these reactive species to pharmaceutical degradation. LID, DCF, and ACT were selected as the model compounds to include one PFA-reactive compound (LID) and two PFA non-reactive compounds (DCF and ACT), with ACT known for its potential susceptibility to R–O$^{\bullet}$ (Table 1). The contribution of reactive species was estimated based on the kinetic rate constants (min^{-1}) obtained under UV-C/PFA+TBA and UV-C/PFA+MeOH, as described in Eqs. (6)–(9).

$$\%UV\text{–}C_{photolysis} = \frac{k_{UV-C}}{k_{UV-C/PFA}} * 100 \quad (6)$$

$$\%HO^{\bullet} = \frac{k_{UV-C/PFA} - k_{UV-C/PFA+TBA}}{k_{UV-C/PFA}} * 100 \quad (7)$$

$$\%R\text{–}O^{\bullet} = \frac{k_{UV-C/PFA+TBA} - k_{UV-C/PFA+MeOH}}{k_{UV-C/PFA}} \quad (8)$$

$$\%otherreactivespecies = 100 - \%UV\text{–}C_{photolysis} - \%HO^{\bullet} - \%R\text{–}O^{\bullet} \quad (9)$$

TBA and MeOH had varying impacts on the three pharmaceuticals (Fig. 5). TBA significantly inhibited the degradation of LID and DCF but had little impact on ACT. The stronger inhibitory effect of MeOH on LID and ACT compared to TBA supports the hypothesis that, in addition to HO$^{\bullet}$, other reactive species played a more significant role in their degradation under UV-C/PFA (Table S1). Accordingly, HO$^{\bullet}$ accounted for 32.9 %, 30.6 %, and 8.9 % of the degradation of LID, DCF, and ACT, respectively (Table S1), while some R–O$^{\bullet}$ (additional radicals quenched by MeOH) contributed 45.6 %, 10.6 %, and 52.5 % to their degradation. In the case of DCF (a photosensitive compound with direct UV-C photolysis contributing at 52.7 %), the results (Table S1) overall corroborate previous findings under UV-C/PAA, where 56.0 % of its degradation was ascribed to direct UV-C photolysis, 32.0 % to HO$^{\bullet}$, and 12.0 % to other organic radicals [75].

Overall, these results (Fig. 5 and Table S1) support the earlier observations (part 3.3.2), where the simultaneous contribution of HO$^{\bullet}$ and R–O$^{\bullet}$ was observed for LID, and that among the three pharmaceuticals, the higher contribution of R–O$^{\bullet}$ was highlighted for ACT. The percentage attributed to other reactive species reflects the contribution of PFA and $^1O_2$ for PFA-reactive compounds (LID), as well as all other reactive species not quenched by MeOH or TBA. In addition, further research is needed to isolate the contribution of $^1O_2$ alone by using other quenching agents, such as sodium azide. However, the lower value of $k_{UV-C/PFA+MeOH}$ for LID, compared to k_{PFA}, is attributed to the decreased availability of PFA for oxidation due to its photolytic decomposition. As a result, it was not possible to quantify the PFA molecule contribution under UV-C/PFA. It is hypothesized, however, that the PFA contribution is less significant under UV-C/PFA than when used alone, primarily due to the high photodegradation of PFA. This consideration is important when applying this AOP in real WWTPs, where using these processes sequentially rather than simultaneously could better leverage PFA's selective reactivity for certain compounds (e.g., LID).

3.3.4. *Influence of the initial pH and identification of transformation products in phosphate buffer solution*

The pH influence was evaluated during the oxidation of LID and DCF by UV-C/PFA (1 μM of pharmaceutical and 500 μM of PFA). For this, the initial pH of the PBS was regulated to five levels: 2.0, 5.0, 7.0, 9.0, and 11.0. In each experiment, the final pH decreased by less than 0.5 units. This broad pH range (2.0–11.0) was selected to assess the influence of pH on the reactivity of UV-C/PFA, considering that the autodecomposition behavior of PFA was previously described across this pH range [46]. Additionally, this pH range encompasses the typical wastewater pH in the Paris region (average pH 7.9 ± 0.1), used here to evaluate pharmaceutical removal under real conditions (Part 3.4).

During the oxidation of LID by UV-C/PFA, as previously observed with its degradation by PFA, the $k_{UV-C/PFA}$ increased with increasing pH (from 2.0 to 8.0, stabilizing up to pH 11.0) due to the predominant presence of the deprotonated forms of both LID and PFA [46]. The analogous pH-dependent behavior in the oxidation of LID by both PFA and UV-C/PFA is primarily due to the significant contribution of the PFA molecule and $^1O_2$ to its degradation under UV-C/PFA (part 3.3.3) compared to other reactive species present in the system. In addition, the

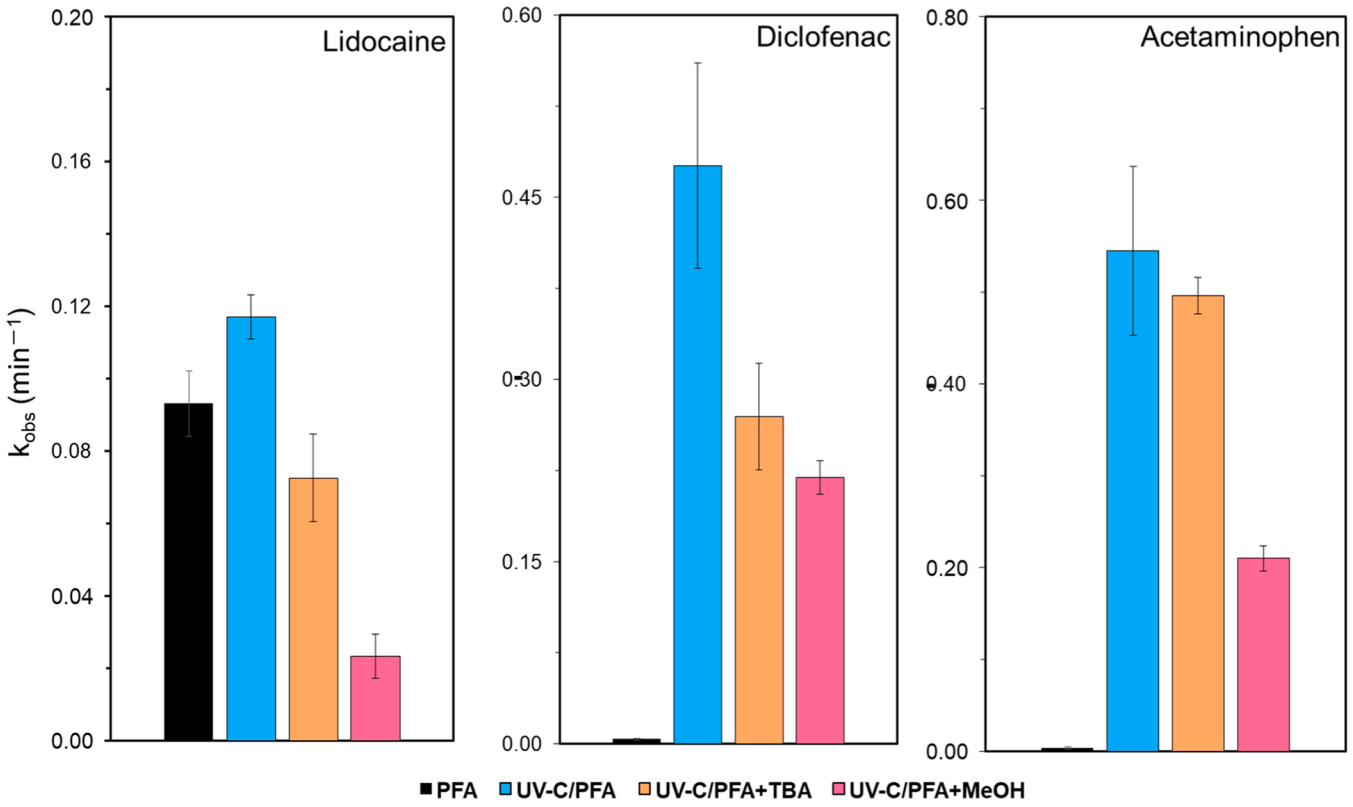

Fig. 5. Contribution of UV-C photolysis, $HO^{\bullet}$, and additional reactive species to the degradation kinetics of lidocaine, diclofenac, and acetaminophen under UV-C/PFA. Experimental conditions: $[pharmaceutical]_0 = 1$ μM, $[PFA]_0 = 500$ μM, [TBA] = [MeOH] = 200 mM, [PBS] = 10 mM, pH 7.1, 20 ± 1 °C, UV-C fluence = 0.5 ± 0.01 $mW.cm^{-2} = 2.3 \pm 0.03 \times 10^{-7}$ $Einstein.L^{-1}.s^{-1}$.

reactivity of DCF under UV-C/PFA increased to a maximum at pH 7.0 and decreased in alkaline conditions (pH > 7.0). The low reactivity of DCF in both acidic and alkaline conditions may be attributed to the consumption of $HO^{\bullet}$, which plays a significant role in the degradation of DCF (30.6 % of the $k_{UV\text{-}C/PFA}$, part 3.3.3) through side reactions with both H^+ and OH^- ions. This phenomenon was previously observed during the degradation of propiconazole, a triazole fungicide, by UV-C/H_2O_2 [28]. A similar behavior was noted in the degradation of DCF by UV/TiO_2, where the authors primarily attributed this effect to the surface charge of TiO_2 [64] rather than the structure or properties of DCF. The recurrence of this phenomenon in UV-C/PFA suggests the need for further investigation into the role of direct UV-C photolysis in relation to DCF properties. Additional insights into the role of pH in the degradation of LID and DCF are discussed in Text S4 and supported by Figure S6.

In addition, to gain a deeper understanding of the oxidation mechanisms of pharmaceuticals by PFA and UV-C/PFA and the pH influence, the TPs generated during the oxidation of LID and DCF in 10 mM PBS (pH 7.0) at five levels of pH ranging from 2.0–11.0 were characterized by high resolution mass spectrometry (HRMS). The exact masses of LID and DCF and their TPs, as well as their detection parameters and main fragments, are described in Tables S2 and S3, and the detailed identifications for each TP at various pH as well as the influence of quenchers (TBA and MeOH) on the TP formation are described in Text S5. A mechanism was proposed when the identification of the TP was possible (Figure S7).

As observed previously for PFA oxidation [46,48], lidocaine N-oxide (*m/z* 251.1755) was the most intense TP under PFA and UV-C/PFA (Table S2). Its higher intensity in alkaline conditions can be related to the higher reactivity of LID in those conditions. For DCF oxidation, no TPs were observed at all pH values under PFA oxidation, likely due to the low oxidation rate of DCF by PFA [46], while seven TPs were detected under UV-C/PFA, some of which corresponded to the loss of a chlorine atom or the carboxylic group (when the identification of the structure was possible, Table S2 and Figure S7). However, due to the inability to propose structures for all the observed TPs, it remains challenging to establish a direct correlation between their exclusive presence and the related pH conditions.

Overall, the TPs formed by PFA oxidation had higher molecular weights compared to those obtained under UV-C/PFA, probably due to the different oxidation mechanisms involved in the two processes and the enhanced oxidation rates obtained with AOPs. UV-C/PFA involves processes like homolytic bond dissociation, photocleavage, and ring cleavage induced by $HO^{\bullet}$ [28,51,67] from the background UV-C/H_2O_2, leading to smaller molar mass TPs, while PFA primarily adds oxygen atoms, resulting in higher molar mass TPs [46].

3.4. Removal of pharmaceuticals by UV-C/PFA in wastewater effluent

To study the impact of UV-C/PFA on pharmaceutical degradation under realistic conditions, six pharmaceuticals were spiked into treated wastewater and then subjected to oxidation at 10 $mg.L^{-1}$ (161 μM) of PFA and 60 min of reaction. Prior to spiking, the analysis of the non-spiked wastewater samples (experiment conducted over three days) revealed the presence of these pharmaceuticals at varying concentrations (C_0), ranging from 0.3 $\mu g.L^{-1}$ for SMX to 1.3 $\mu g.L^{-1}$ for DCF. In one sample, FUR and ACT were detected at 3.4 $\mu g.L^{-1}$ and 16.7 $\mu g.L^{-1}$, respectively.

As expected (based on the $k_{UV\text{-}C/PFA}$ of pharmaceuticals compared to k_{PFA}, Table 1), UV-C/PFA increased the removal rates of all pharmaceuticals (Fig. 6), ranging from 10.9 ± 2.5 % for CBZ to 76.1 ± 5.5 % for DCF. These removal rates were consistent with the $k_{UV\text{-}C/PFA}$ results (part 3.3.2), which placed DCF among the most reactive compounds, CBZ as the least reactive compound and a slight difference (only 20.0 %) was

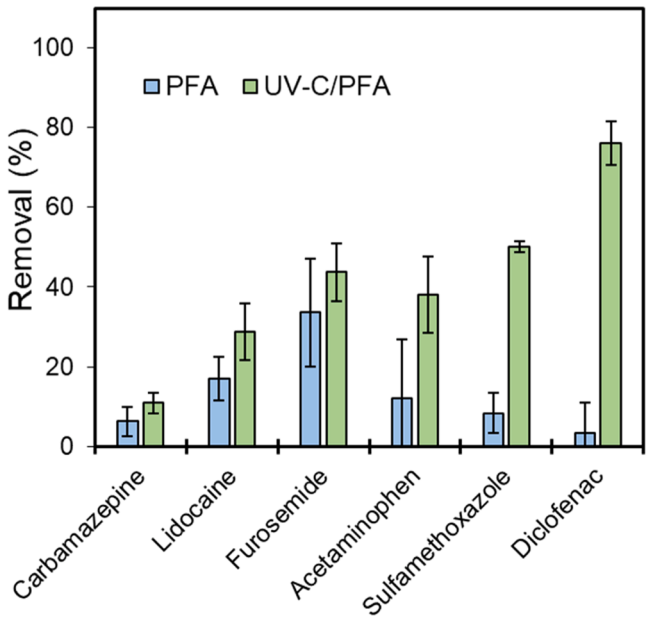

Fig. 6. The removal rate of pharmaceuticals in wastewater effluent by UV-C/PFA and PFA (data obtained from Nabintu Kajoka et al., [46]). Experimental conditions: $[Pharmaceutical]_0 = C_0 + 1.0\ \mu g.L^{-1}$ spiked in wastewater effluent, with C_0 the initial concentration of the pharmaceutical in the wastewater effluent, reaction time = 60 min, pH = 7.9 ± 0.1, 20.0°C, $[PFA]_0 = 10\ mg.L^{-1} = 161\ \mu M$, and UV-C fluence $= 0.5 \pm 0.01\ mW.cm^{-2} = 2.3 \pm 0.03 \times 10^{-7}$ $Einstein.L^{-1}.s^{-1}$. Error bars represent the standard deviation from triplicate samples.

observed between the reactivity of LID under PFA and UV-C/PFA. For the oxidation by PFA, the maximum removal rate observed for these six compounds was 33.6 ± 13.6 % for FUR [46]. All the observed removal rates, however, were lower than expected. In kinetic experiments in PBS, four pharmaceuticals (DCF, SMX, ACT, and FUR) were completely degraded by 31 mg. L^{-1} (500 μM) of PFA in less than 5 min. The fact that none of these pharmaceuticals were completely removed within 60 min when spiked in wastewater effluent indicates that, as previously observed for PFA [46], their removal rate was hindered by wastewater constituents, such as total suspended solids, dissolved organic matter, alkalinity or dissolved salts.

4. Conclusion

This study investigated, for the first time, the degradation kinetics of six pharmaceuticals by UV-C/PFA. A synergistic effect was observed between UV-C photolysis and PFA, significantly enhancing the removal rate of all pharmaceuticals in PBS or wastewater effluent compared to PFA alone. This improved degradation resulted from different reactive species, including $^1O_2$, $HCOO^•$, $HCOOO^•$ and $HO^•$, with $HO^•$ originating principally from the background UV-C/H_2O_2. Although UV-C/PFA does not generate more $HO^•$ than UV-C/H_2O_2 (a common AOP), it offers an advantage due to the significant additional contribution of $R–O^•$ and $^1O_2$ in the degradation of some pharmaceuticals (LID, FUR, SMX, and ACT). The contribution of reactive species to the degradation of pharmaceuticals was investigated, but supplementary quenching experiments with sodium azide and the determination of the steady-state concentration of $^1O_2$ should be performed to distinguish the role of the PFA molecule from that of $^1O_2$, as the latter appears to be the most reactive species in PFA oxidation. Nevertheless, the contribution of PFA to the degradation of PFA-reactive molecules (e.g., LID, FUR) under UV-C/PFA is lower than when PFA is used alone. Therefore, determining the optimal sequence for coupling the two processes is crucial to maximize their benefits. For instance, a first reactor could be used for PFA disinfection and reaction with PFA-reactive molecules, followed by a second UV-C reactor in series to perform an AOP with the residual PFA for treating more recalcitrant pharmaceuticals. In wastewater effluent, UV-C/PFA increased the removal rate of all pharmaceuticals compared to PFA. However, the removal rates were lower than expected (based on their $k_{UV\text{-}C/PFA}$) due to scavenging effects from wastewater constituents such as total suspended solids, alkalinity, organic matter, or dissolved salts. The insights gained from this study provide a valuable foundation for further research on UV-C/PFA and other PFA-based AOPs. Future investigations could focus on the impact of wastewater constituents, as well as the toxicity of oxidized waters and TPs compared to other AOPs, which would advance the development of UV-C/PFA as a novel strategy for micropollutant removal in water treatment. Despite the promising results of UV-C/PFA, the addition of UV-C photolysis increases electrical consumption. Therefore, techno-economic assessments are necessary to demonstrate the feasibility and advantages of this novel AOP.

Environmental implication

Performic acid (PFA) is an innovative disinfectant effective in removing pathogenic microorganisms, including *Escherichia coli*, enterococci, and viruses, from wastewater. However, due to its limited and selective reactivity with pharmaceuticals, PFA requires activation to target these contaminants effectively. In this study, PFA was combined with UV-C photolysis to create an advanced oxidation process (UV-C/PFA) that enhances pharmaceutical degradation by generating reactive species, such as hydroxyl and peroxyl radicals, and singlet oxygen. These results indicate the potential to extend PFA's role beyond disinfection, utilizing it as an oxidant to treat a broader range of emerging contaminants in wastewater.

CRediT authorship contribution statement

Diop Yacine Khadija: Formal analysis. **Chebbo Ghassan:** Funding acquisition. **Gasperi Johnny:** Writing – review & editing, Conceptualization, Validation, Supervision. **Oliveira Marcos:** Validation, Supervision, Writing – review & editing, Conceptualization. **Vincent Rocher:** Funding acquisition. **Christelle Nabintu Kajoka:** Writing – original draft, Conceptualization, Investigation, Methodology. **Le Roux Julien:** Supervision, Conceptualization, Writing – review & editing, Validation. **Brosillon Stephan:** Validation, Conceptualization, Writing – review & editing, Supervision. **Reibel Corine:** Formal analysis.

Declaration of Competing Interest

The authors declare that they have no known competing financial interests or personal relationships that could have appeared to influence the work reported in this paper.

Acknowledgments

The authors thank the OPUR and WaterOmics (ANR-17-CE34-0009–01) research programs for their financial support. We are grateful to the PRAMMICS Platform (OSU-EFLUVE UMS 3563) for their assistance with UPLC-IMS-QTOF and HPLC-DAD analyses. We also thank Florian Huet for his assistance in building the UV-C photolysis system, as well as Emilie Caupos, Emmanuelle Mebold, Lila Boudhamane, Melissia Ben-Iken, and Ilyess Taibi for their contributions to various experiments and analyses. Finally, we thank Gabson Baguma (University of Nevada) for improving the clarity and quality of the manuscript.

Appendix A. Supporting information

Supplementary data associated with this article can be found in the online version at doi:10.1016/j.jhazmat.2025.139016.

Data availability

Data will be made available on request.

References

[1] Alvarez, M.N., Peluffo, G., Folkes, L., Wardman, P., Radi, R., 2007. Reaction of the carbonate radical with the spin-trap 5,5-dimethyl-1-pyrroline-*N*-oxide in chemical and cellular systems: Pulse radiolysis, electron paramagnetic resonance, and kinetic-competition studies. Free Radic Biol Med 43, 1523–1533. https://doi.org/10.1016/j.freeradbiomed.2007.08.002.

[2] Ao, X., Wang, W., Sun, W., Lu, Z., Li, C., 2021. Degradation and transformation of norfloxacin in medium-pressure ultraviolet/peracetic acid process: An investigation of the role of pH. Water Res 203, 117458. https://doi.org/10.1016/j.watres.2021.117458.

[3] Appiani, E., Ossola, R., Latch, D.E., Erickson, P.R., McNeill, K., 2017. Aqueous singlet oxygen reaction kinetics of furfuryl alcohol: effect of temperature, pH, and salt content. Environ Sci Process Impacts 19, 507–516. https://doi.org/10.1039/C6EM00646A.

[4] Baldry, M.G.C., 1983. The bactericidal, fungicidal and sporicidal properties of hydrogen peroxide and peracetic acid. J Appl Bacteriol 54, 417–423. https://doi.org/10.1111/j.1365-2672.1983.tb02637.x.

[5] Bolton, J.R., Cater, S., 1994. Homog Photo Pollut Contam Water Introd 467–490. https://doi.org/10.1201/9781351069847-35.

[6] Boxall, A.B.A., 2004. The environmental side effects of medication. EMBO Rep 5, 1110–1116. https://doi.org/10.1038/sj.embor.7400307.

[7] Buxton, G.V., Greenstock, C.L., Helman, W.P., Ross, A.B., 1988. Critical Review of rate constants for reactions of hydrated electrons, hydrogen atoms and hydroxyl radicals (·OH/·O− in Aqueous Solution. J Phys Chem Ref Data 17, 513–886. https://doi.org/10.1063/1.555805.

[8] Cai, M., Sun, P., Zhang, L., Huang, C.-H., 2017. UV/Peracetic acid for degradation of pharmaceuticals and reactive species evaluation. Environ Sci Technol 51, 14217–14224. https://doi.org/10.1021/acs.est.7b04694.

[9] Cai, Z., Liu, W., Fu, J., O'Reilly, S.E., Zhao, D., 2017. Effects of oil dispersants on photodegradation of parent and alkylated anthracene in seawater. Environ Pollut 229, 272–280. https://doi.org/10.1016/j.envpol.2017.05.084.

[10] Campo, N., De Flora, C., Maffettone, R., Manoli, K., Sarathy, S., Santoro, D., Gonzalez-Olmos, R., Auset, M., 2020. Inactivation kinetics of antibiotic resistant Escherichia coli in secondary wastewater effluents by peracetic and performic acids. Water Res 169, 115227. https://doi.org/10.1016/j.watres.2019.115227.

[11] Can-Güven, E., Daniser, Y., Yazici Guvenc, S., Ghanbari, F., Varank, G., 2022. Effective removal of furfural by ultraviolet activated persulfate, peroxide, and percarbonate oxidation: Focus on influencing factors, kinetics, and water matrix effect. J Photochem Photobiol A Chem 433, 114139. https://doi.org/10.1016/j.jphotochem.2022.114139.

[12] Cavallini, G.S., Campos, S.X., de, Souza, J.B., de, Vidal, C.M., de, S., 2013. Comparison of methodologies for determination of residual peracetic acid in wastewater disinfection. Int J Environ Anal Chem 93, 906–918. https://doi.org/10.1080/03067319.2012.702274.

[13] Chen, H., Wang, J., 2021. Degradation and mineralization of ofloxacin by ozonation and peroxone (O3/H2O2) process. Chemosphere 269, 128775. https://doi.org/10.1016/j.chemosphere.2020.128775.

[14] Chen, L., Yamane, S., Mizukado, J., Suzuki, Y., Kutsuna, S., Uchimaru, T., Suda, H., 2015. ESR study of singlet oxygen generation and its behavior during the photo-oxidation of P3HT in solution. Chem Phys Lett 624, 87–92. https://doi.org/10.1016/j.cplett.2015.02.019.

[15] Chen, S., Cai, M., Liu, Y., Zhang, L., Feng, L., 2019. Effects of water matrices on the degradation of naproxen by reactive radicals in the UV/peracetic acid process. Water Res 150, 153–161. https://doi.org/10.1016/j.watres.2018.11.044.

[16] Chen, Z., Teng, Y., Wang, W., Hong, R., Huang, L., Wang, X., Zhu, F., Li, H., Hao, S., Wu, B., Gu, C., 2022. Enhanced UV photoreductive destruction of perfluorooctanoic acid in the presence of alcohols: Synergistic mechanism of hydroxyl radical quenching and solvent effect. Appl Catal B Environ 316, 121652. https://doi.org/10.1016/j.apcatb.2022.121652.

[17] Clennan, E.L., Pace, A., 2005. Advances in singlet oxygen chemistry. Tetrahedron 61, 6665–6691. https://doi.org/10.1016/j.tet.2005.04.017.

[18] Deng, J., Wang, H., Fu, Y., Liu, Y., 2022. Phosphate-induced activation of peracetic acid for diclofenac degradation: Kinetics, influence factors and mechanism. Chemosphere 287, 132396. https://doi.org/10.1016/j.chemosphere.2021.132396.

[19] Deng, S., Yang, Z., Yu, X., Li, M., Cao, H., 2024. The reactivity of organic radicals in the performic, peracetic, perpropionic acids-based advanced oxidation process: A case study of sulfamethoxazole. J Hazard Mater 476, 135033. https://doi.org/10.1016/j.jhazmat.2024.135033.

[20] Fontmorin, J.M., Burgos Castillo, R.C., Tang, W.Z., Sillanpää, M., 2016. Stability of 5,5-dimethyl-1-pyrroline-*N*-oxide as a spin-trap for quantification of hydroxyl radicals in processes based on Fenton reaction. Water Res 99, 24–32. https://doi.org/10.1016/j.watres.2016.04.053.

[21] Gagnon, C., Lajeunesse, A., Cejka, P., Gagné, F., Hausler, R., 2008. Degradation of Selected Acidic and Neutral Pharmaceutical Products in a Primary-Treated Wastewater by Disinfection Processes. Ozone Science Engineering 30, 387–392. https://doi.org/10.1080/01919510802336731.

[22] Gehr, R., Chen, D., Moreau, M., 2009. Performic acid (PFA): tests on an advanced primary effluent show promising disinfection performance. Water Sci Technol 59, 89–96. https://doi.org/10.2166/wst.2009.761.

[23] Gomes, A., Fernandes, E., Lima, J.L.F.C., 2005. Fluorescence probes used for detection of reactive oxygen species. J Biochem Biophys Methods 65, 45–80. https://doi.org/10.1016/j.jbbm.2005.10.003.

[24] Guillossou, R., Le Roux, J., Mailler, R., Vulliet, E., Morlay, C., Nauleau, F., Gasperi, J., Rocher, V., 2019. Organic micropollutants in a large wastewater treatment plant: What are the benefits of an advanced treatment by activated carbon adsorption in comparison to conventional treatment? Chemosphere 218, 1050–1060. https://doi.org/10.1016/j.chemosphere.2018.11.182.

[25] Guzzella, L., Monarca, S., Zani, C., Feretti, D., Zerbini, I., Buschini, A., Poli, P., Rossi, C., Richardson, S.D., 2004. In vitro potential genotoxic effects of surface drinking water treated with chlorine and alternative disinfectants. Mutat Res/Genet Toxicol Environ Mutagen 564, 179–193. https://doi.org/10.1016/j.mrgentox.2004.08.006.

[26] Halladja, S., ter Halle, A., Aguer, J.-P., Boulkamh, A., Richard, C., 2007. Inhibition of Humic Substances Mediated Photooxygenation of Furfuryl Alcohol by 2,4,6-Trimethylphenol. Evidence for Reactivity of the Phenol with Humic Triplet Excited States. Environ Sci Technol 41, 6066–6073. https://doi.org/10.1021/es070656t.

[27] Hollman, J., Dominic, J.A., Achari, G., 2020. Degradation of pharmaceutical mixtures in aqueous solutions using UV/peracetic acid process: Kinetics, degradation pathways and comparison with UV/H2O2. Chemosphere 248, 125911. https://doi.org/10.1016/j.chemosphere.2020.125911.

[28] Hong, A.-J., Lee, J., Cha, Y., Zoh, K.-D., 2022. Propiconazole degradation and its toxicity removal during UV/H2O2 and UV photolysis processes. Chemosphere 302, 134876. https://doi.org/10.1016/j.chemosphere.2022.134876.

[29] Huang, Y., Kong, M., Coffin, S., Cochran, K.H., Westerman, D.C., Schlenk, D., Richardson, S.D., Lei, L., Dionysiou, D.D., 2020. Degradation of contaminants of emerging concern by UV/H2O2 for water reuse: Kinetics, mechanisms, and cytotoxicity analysis. Water Res 174, 115587. https://doi.org/10.1016/j.watres.2020.115587.

[30] Huynh, N., Caupos, E., Peirera, C., Le Roux, J., Bressy, A., Moilleron, R., 2021. Evaluation of sample preparation methods for non-target screening of organic micropollutants in urban waters using high-resolution mass spectrometry. Molecules 26, 7064. https://doi.org/10.3390/molecules26237064.

[31] Karpova, T., Pekonen, P., Gramstad, R., Öjstedt, U., Laborda, S., Heinonen-Tanski, H., Chávez, A., Jiménez, B., 2013. Performic acid for advanced wastewater disinfection. Water Sci Technol 68, 2090–2096. https://doi.org/10.2166/wst.2013.468.

[32] Kim, J., Du, P., Liu, W., Luo, C., Zhao, H., Huang, C.-H., 2020. Cobalt/peracetic acid: advanced oxidation of aromatic organic compounds by acetylperoxyl radicals. Environ Sci Technol 54, 5268–5278. https://doi.org/10.1021/acs.est.0c00356.

[33] Kim, J., Zhang, T., Liu, W., Du, P., Dobson, J.T., Huang, C.-H., 2019. Advanced oxidation process with peracetic acid and Fe(II) for contaminant degradation. Environ Sci Technol 53, 13312–13322. https://doi.org/10.1021/acs.est.9b02991.

[34] Kitis, M., 2004. Disinfection of wastewater with peracetic acid: a review. Environ Int 30, 47–55. https://doi.org/10.1016/S0160-4120(03)00147-8.

[35] Liao, Q.-N., Ji, F., Li, J.-C., Zhan, X., Hu, Z.-H., 2016. Decomposition and mineralization of sulfaquinoxaline sodium during UV/H2O2 oxidation processes. Chem Eng J 284, 494–502. https://doi.org/10.1016/j.cej.2015.08.150.

[36] Lin, H.H.-H., Lin, A.Y.-C., 2024. Peracetic acid as an alternative disinfectant for micropollutants degradation and disinfection byproducts control in outdoor swimming pools. J Hazard Mater 464, 132988. https://doi.org/10.1016/j.jhazmat.2023.132988.

[37] Lin, J., Hu, Y., Xiao, J., Huang, Y., Wang, M., Yang, H., Zou, J., Yuan, B., Ma, J., 2021. Enhanced diclofenac elimination in Fe(II)/peracetic acid process by promoting Fe(III)/Fe(II) cycle with ABTS as electron shuttle. Chem Eng J 420, 129692. https://doi.org/10.1016/j.cej.2021.129692.

[38] Lubello, C., Caretti, C., Gori, R., 2002. Comparison between PAA/UV and H2O2/UV disinfection for wastewater reuse. Water Supply 2, 205–212. https://doi.org/10.2166/ws.2002.0025.

[39] Luukkonen, T., Heyninck, T., Rämö, J., Lassi, U., 2015. Comparison of organic peracids in wastewater treatment: Disinfection, oxidation and corrosion. Water Res 85, 275–285. https://doi.org/10.1016/j.watres.2015.08.037.

[40] Meyer, E., 1976. [Disinfection of sewage waters from rendering plants by means by peracetic acid]. J Hyg Epidemiol Microbiol Immunol 21, 266–273.

[41] Min, D.B., Boff, J.M., 2002. Chemistry and reaction of singlet oxygen in foods. Compr Rev Food Sci Food Saf 1, 58–72. https://doi.org/10.1111/j.1541-4337.2002.tb00007.x.

[42] Mitch, W.A., Sharp, J.O., Trussell, R.R., Valentine, R.L., Alvarez-Cohen, L., Sedlak, D.L., 2003. Nitrosodimethylamine (NDMA) as a Drinking Water Contaminant: A Review. Environ Eng Sci 20, 389–404. https://doi.org/10.1089/109287503768335896.

[43] Miyamoto, S., Martinez, G.R., Martins, A.P.B., Medeiros, M.H.G., Di Mascio, P., 2003. Direct Evidence of Singlet Molecular Oxygen [O_2 ($^1\Delta_g$)] Production in the Reaction of Linoleic Acid Hydroperoxide with Peroxynitrite. J Am Chem Soc 125, 4510–4517. https://doi.org/10.1021/ja029262m.

[44] Miyamoto, S., Martinez, G.R., Medeiros, M.H.G., Di Mascio, P., 2003. Singlet Molecular Oxygen Generated from Lipid Hydroperoxides by the Russell Mechanism: Studies Using^{18} O-Labeled Linoleic Acid Hydroperoxide and Monomol Light Emission. Meas J Am Chem Soc 125, 6172–6179. https://doi.org/10.1021/ja029115o.

[45] Moan, J., Wold, E., 1979. Detection of singlet oxygen production by ESR. Nature 279, 450–451. https://doi.org/10.1038/279450a0.

[46] Nabintu Kajoka, C., Gasperi, J., Brosillon, S., Caupos, E., Mebold, E., Oliveira, M., Rocher, V., Chebbo, G., Le Roux, J., 2023. Reactivity of performic acid with

organic and inorganic compounds: from oxidation kinetics to reaction pathways. ACS EST Water. https://doi.org/10.1021/acsestwater.3c00279.
[47] Nabintu Kajoka, C., Oliveira, M., Ba, W., Giroud, B., Vulliet, E., Caupos, E., Chebbo, G., Guérin, S., Rocher, V., Gasperi, J., Le Roux, J., Brosillon, S., 2025. Utilisation de l'acide performique pour réduire la pollution microbiologique et chimique des eaux résiduaires urbaines. Tech Sci Méthodes. https://doi.org/10.36904/tsm/202412195.
[48] Nihemaiti, M., Huynh, N., Mailler, R., Mèche-Ananit, P., Rocher, V., Barhdadi, R., Moilleron, R., Le Roux, J., 2022. High-Resolution Mass Spectrometry Screening of Wastewater Effluent for Micropollutants and Their Transformation Products during Disinfection with Performic Acid. ACS EST. Water 2, 1225–1233. https://doi.org/10.1021/acsestwater.2c00075.
[49] Paillard, H., Brunet, R., Dore, M., 1988. Conditions optimales d'application du systeme oxydant ozone-peroxyde d'hydrogene. Water Res 22, 91–103. https://doi.org/10.1016/0043-1354(88)90135-2.
[50] Plewa, M.J., Wagner, E.D., Muellner, M.G., Hsu, K.-M., Richardson, S.D., 2008. Comparative Mammalian cell toxicity of N-DBPs and C-DBPs. In: Disinfection By-Products in Drinking Water, ACS Symposium Series. American Chemical Society, pp. 36–50. https://doi.org/10.1021/bk-2008-0995.ch003.
[51] Porcar-Santos, O., Cruz-Alcalde, A., Sans, C., 2024. Hydroxyl radical and UV-induced reactions of bisphenol analogues in water: kinetics, transformation products and estrogenic activity estimation. Sci Total Environ 906, 167490. https://doi.org/10.1016/j.scitotenv.2023.167490.
[52] Qiu, W., Zheng, M., Sun, J., Tian, Y., Fang, M., Zheng, Y., Zhang, T., Zheng, C., 2019. Photolysis of enrofloxacin, pefloxacin and sulfaquinoxaline in aqueous solution by UV/H2O2, UV/Fe(II), and UV/H2O2/Fe(II) and the toxicity of the final reaction solutions on zebrafish embryos. Sci Total Environ 651, 1457–1468. https://doi.org/10.1016/j.scitotenv.2018.09.315.
[53] Ragazzo, P., Chiucchini, N., Piccolo, V., Spadolini, M., Carrer, S., Zanon, F., Gehr, R., 2020. Wastewater disinfection: long-term laboratory and full-scale studies on performic acid in comparison with peracetic acid and chlorine. Water Res 184, 116169. https://doi.org/10.1016/j.watres.2020.116169.
[54] Rayaroth, M.P., Aravind, U.K., Boczkaj, G., Aravindakumar, C.T., 2023. Singlet oxygen in the removal of organic pollutants: an updated review on the degradation pathways based on mass spectrometry and DFT calculations. Chemosphere 345, 140203. https://doi.org/10.1016/j.chemosphere.2023.140203.
[55] Rigaudy, J., Breliere, C., Scribe, P., 1978. Photochemistry of 9,10-diphenylanthracene endoperoxide. Tetrahedron Lett 19, 687–690. https://doi.org/10.1016/S0040-4039(01)85367-3.
[56] Rocher, V., Azimi, S. (Eds.), 2021. Effectiveness of Disinfecting Wastewater Treatment Plant Discharges: Case of chemical disinfection using performic acid. IWA Publishing. https://doi.org/10.2166/9781789062106.
[57] Rokhina, E.V., Makarova, K., Golovina, E.A., Van As, H., Virkutyte, J., 2010. Free Radical Reaction Pathway, Thermochemistry of Peracetic Acid Homolysis, and Its Application for Phenol Degradation: Spectroscopic Study and Quantum Chemistry Calculations. Environ Sci Technol 44, 6815–6821. https://doi.org/10.1021/es1009136.
[58] Rosenfeldt, E.J., Linden, K.G., 2007. The $R_{OH,UV}$ Concept to Characterize and the Model UV/H_2O_2 Process in Natural Waters. Environ Sci Technol 41, 2548–2553. https://doi.org/10.1021/es062353p.
[59] Santacesaria, E., Russo, V., Tesser, R., Turco, R., Di Serio, M., 2017. Kinetics of performic acid synthesis and decomposition. Ind Eng Chem Res 56, 12940–12952. https://doi.org/10.1021/acs.iecr.7b00593.
[60] Shi, H.-C., Li, Y., 2007. Formation of nitroxide radicals from secondary amines and peracids: A peroxyl radical oxidation pathway derived from electron spin resonance detection and density functional theory calculation. J Mol Catal A Chem 271, 32–41. https://doi.org/10.1016/j.molcata.2007.02.012.
[61] Sun, X., Zhao, X., Du, W., Liu, D., 2011. Kinetics of Formic Acid-autocatalyzed Preparation of Performic Acid in Aqueous Phase. Chin J Chem Eng 19, 964–971. https://doi.org/10.1016/S1004-9541(11)60078-5.
[62] Tanaka, K., Miura, T., Umezawa, N., Urano, Y., Kikuchi, K., Higuchi, T., Nagano, T., 2001. Rational design of fluorescein-based fluorescence probes. mechanism-based design of a maximum fluorescence probe for singlet. Oxyg J Am Chem Soc 123, 2530–2536. https://doi.org/10.1021/ja0035708.
[63] Teodosiu, C., Gilca, A.-F., Barjoveanu, G., Fiore, S., 2018. Emerging pollutants removal through advanced drinking water treatment: A review on processes and environmental performances assessment. J Clean Prod 197, 1210–1221. https://doi.org/10.1016/j.jclepro.2018.06.247.
[64] Tra, V.T., Pham, V.T., Tran, T.-D., Tran, T.H., Tran, T.K., Nguyen, T.P.T., Nguyen, V.T., Dao, T.-V.-H., Tran, P.-Y.-N., Le, V.-G., Tran, C.-S., 2023. Enhance diclofenac removal in wastewater by photocatalyst process combination with hydrogen peroxide. Case Stud Chem Environ Eng 8, 100506. https://doi.org/10.1016/j.cscee.2023.100506.
[65] Wang, J., Wang, Z., Cheng, Y., Cao, L., Bai, F., Yue, S., Xie, P., Ma, J., 2021. Molybdenum disulfide (MoS2): A novel activator of peracetic acid for the degradation of sulfonamide antibiotics. Water Res 201, 117291. https://doi.org/10.1016/j.watres.2021.117291.
[66] Wang, Z., Fu, Y., Peng, Y., Wang, S., Liu, Y., 2021. HCO3–/CO32– enhanced degradation of diclofenac by Cu(II)-activated peracetic acid: Efficiency and mechanism. Sep Purif Technol 277, 119434. https://doi.org/10.1016/j.seppur.2021.119434.
[67] Wang, Z., Li, C., Wang, Y., Chen, Z., Wang, M., Shi, H., 2023. Photolysis of the novel meta-diamide insecticide broflanilide in solutions: Kinetics, degradation pathway, DFT calculation and ecotoxicity assessment. Chemosphere 320, 138060. https://doi.org/10.1016/j.chemosphere.2023.138060.
[68] Yan, T., Ping, Q., Zhang, A., Wang, L., Dou, Y., Li, Y., 2021. Enhanced removal of oxytetracycline by UV-driven advanced oxidation with peracetic acid: Insight into the degradation intermediates and N-nitrosodimethylamine formation potential. Chemosphere 274, 129726. https://doi.org/10.1016/j.chemosphere.2021.129726.
[69] Yang, W., Zhou, H., Cicek, N., 2014. Treatment of Organic Micropollutants in Water and Wastewater by UV-Based Processes: A Literature Review. Crit Rev Environ Sci Technol 44, 1443–1476. https://doi.org/10.1080/10643389.2013.790745.
[70] Yao, K., Fang, L., Liao, P., Chen, H., 2023. Ultrasound-activated peracetic acid to degrade tetracycline hydrochloride: Efficiency and mechanism. Sep Purif Technol 306, 122635. https://doi.org/10.1016/j.seppur.2022.122635.
[71] Yolchuyeva, U., Jafarova, R., Khamiyev, M., Vakhshouri, A.R., Khamiyeva, G., 2021. Investigation of photochemical conversion processes in aromatic hydrocarbons of Balakhani oil. J Pet Sci Eng 196, 108089. https://doi.org/10.1016/j.petrol.2020.108089.
[72] Yuan, Z., Ni, Y., Van Heiningen, A.R.P., 1997. Kinetics of peracetic acid decomposition: Part I: Spontaneous decomposition at typical pulp bleaching conditions. Can J Chem Eng 75, 37–41. https://doi.org/10.1002/cjce.5450750108.
[73] Zhang, L., Chen, J., Zhang, Y., Xu, Y., Zheng, T., Zhou, X., 2022. Highly efficient activation of peracetic acid by nano-CuO for carbamazepine degradation in wastewater: The significant role of H2O2 and evidence of acetylperoxy radical contribution. Water Res 216, 118322. https://doi.org/10.1016/j.watres.2022.118322.
[74] Zhang, L., Chen, J., Zhang, Y., Yu, Z., Ji, R., Zhou, X., 2021. Activation of peracetic acid with cobalt anchored on 2D sandwich-like MXenes (Co@MXenes) for organic contaminant degradation: High efficiency and contribution of acetylperoxyl radicals. Appl Catal B Environ 297, 120475. https://doi.org/10.1016/j.apcatb.2021.120475.
[75] Zhang, L., Liu, Y., Fu, Y., 2020. Degradation kinetics and mechanism of diclofenac by UV/peracetic acid. RSC Adv 10, 9907–9916. https://doi.org/10.1039/D0RA00363H.
[76] Zhang, T., Huang, C.-H., 2020. Modeling the Kinetics of UV/Peracetic Acid Advanced Oxidation Process. Environ Sci Technol 54, 7579–7590. https://doi.org/10.1021/acs.est.9b06826.
[77] Zhang, X., Yao, J., Zhao, Z., Liu, J., 2019. Degradation of haloacetonitriles with UV/peroxymonosulfate process: degradation pathway and the role of hydroxyl radicals. Chem Eng J 364, 1–10. https://doi.org/10.1016/j.cej.2019.01.029.
[78] Zhao, S., Xue, S., Zhang, J., Zhang, Z., Sun, J., 2020. Dissolved organic matter-mediated photodegradation of anthracene and pyrene in water. Sci Rep 10, 3413. https://doi.org/10.1038/s41598-020-60326-6.